NTNU

Norwegian University of
Science and Technology

Corrosion and Cathodic Protection of PMM Propellers

Simen Hartvigsen

Master of Science in Mechanical Engineering
Submission date: June 2018
Supervisor: Roy Johnsen, MTP
Co-supervisor: Hedda Nordby Krogstad, Brunvoll

Norwegian University of Science and Technology
Department of Mechanical and Industrial Engineering

Preface

This thesis is submitted in partial fulfillment of the requirements for degree Master of Science (MSc) for the Department of Mechanical and Industrial Engineering (MTP) at the Norwegian University of Science and Technology (NTNU).

This thesis is continued work of my project in the course TMM4560 - *Engineering Design and Materials, Specialization Project*.

I would like to thank my supervisor, Professor Roy Johnsen for continued support and guidance. Your help with theoretical and practical assistance was crucial for the production of this report. I would also like to thank Hedda Nordby Krogstad for her encouragement and inspiration, and her tips on how to start this project.

Without the assistance of Børge Holen with production and modification of the test cell, the final result would not have been the same. Many hours were put into the production of the final test cell, and many hours were put into the preparation of the samples prior to testing, and with the support of Nils-Inge Johan Nilsen, this process went far smoother than expected. I would also like to thank Cristian Torres Rodriguez for his assistance with the oxygen measurements.

Simen Dyrstad Hartvigsen

Abstract

This thesis will examine the effect of water flow on cathodic protection (CP) of AISI 316L Stainless Steel (SS) and Nickel-Aluminium bronze (NAB). It will also examine the effect water flow has on the galvanic current of these metals. The SS and NAB are fitted to a structure inside a geometrically confined gap, and CP of these metals will be investigated with special regard to the potential drop through the confined gap. There will be conducted three experimental tests; CP without flow, CP with flow and galvanic couple with flow. A multiphysics modeling program called COMSOL will then be used to simulate the same scenarios using polarization curves collected after each test as boundary conditions. The first two tests will have a special regard to whether CP will be able to protect the metals through the gap. The third test will examine the effect of water flow on galvanic corrosion. The objective is to test whether or not CP can protect the metal surfaces through the confined gap with and without water flow. An aluminium sacrificial anode was used for the first experiment, and was placed outside of the test cell. The corrosion potential of the aluminium anode was -1,064V vs. Ag/AgCl, and the potential of the electrode surface in the middle of the test cell, which is furthest from the anode, was -0,96V vs. Ag/AgCl. This is a potential drop of 104mV, and the potential inside the test cell is sufficient to cathodically protect the metal surfaces. For the second test, a potentiostat was used and applied a potential of -1,050V vs. Ag/AgCl. The potential of the sample furthest away from the anode was measured at -0,42V vs. Ag/AgCl. According to ISO 12473:2017, this potential is not sufficient enough to cathodically protect the surfaces inside the test cell. A COMSOL model was used with polarization curves recorded after each of these tests as boundary conditions. This model showed that the largest potential drop occurred through the first segment, which had the smallest cross-sectional area for the seawater to pass through, which also has the highest fluid resistance. The model also showed similar current densities as was measured during testing, and similar electrode potentials inside the test cell. The third test was a galvanic couple between SS and NAB. Test 3 shows the behaviour of the galvanic couple, and measures the current production from the less noble metal (NAB), and the current consumption of the noble metal (SS). Over time, corrosion products developed on the surface. These corrosion products have not been examined but compared to similar results in literature. The assumption is that with higher water speeds these deposits will be removed, and the effect of galvanic corrosion will decrease.

Keywords: Nickel Aluminium bronze (NAB), AISI 316L Stainless Steel (SS), Cathodic Protection (CP), galvanic current, water flow, confined geometry, natural seawater, permanent magnet motors (PMM).

Sammendrag

Denne oppgaven vil undersøke effekten av vannstrøm på katodisk beskyttelse av AISI 316L Stainless Steel (SS) og Nikkel-Aluminium Bronse (NAB). Denne avhandlingen vil også undersøke effekten vannstrømmen har på galvanisk strøm av de samme metallene. SS og NAB er montert på en struktur inne i et geometrisk begrenst rom, og katodisk beskyttelse av disse metallene vil bli undersøkt med spesielt hensyn til potensialet gjennom det begrensede rommet. Det vil bli gjennomført tre eksperimentelle tester; katodisk beskyttelse uten vannstrøm, katodisk beskyttelse med vannstrøm og galvanisk korrosjon med vannstrøm. Et multi fysisk modellerings porgram kalt COMSOL vil bli brukt til å simulere de samme scenarioene ved hjelp av polarisasjonskurver hentet etter hver test som grensebetingelser. De to første testene vil ha et spesielt hensyn til hvorvidt katodisk beskyttelse vil ha muligheten til å beskytte metallene gjennom det begrensede rommet. Den tredje testen vil undersøke effekten av vannstrøm på galvanisk korrosjon. Målet er å teste hvorvidt CP kan beskytte metallflatene gjennom det begrensede rommet med og uten vannstrømning. En aluminium offeranode ble brukt til det første eksperimentet, og ble plassert utenfor testcellen. Korrosjonspotensialet til aluminiumanoden var -1,064V mot Ag/AgCl, og potensialet til elektrodeoverflaten i midten av testcellen, som er lengst unna anoden, var -0,96V mot Ag/AgCl. Dette viser en potensialtap på 104mV, og beskyttelsespotensialet i testcellen er tilstrekkelig til å beskytte metalloverflatene katodisk. For den andre testen ble en potensiostat brukt, og tilført et potensial på -1,050V mot Ag/AgCl. Potensialet av prøven lengst vekk fra anoden ble målt ved -0,42V mot Ag/AgCl. I henhold til ISO 12473:2017 er ikke dette potensialet tilstrekkelig til å beskytte overflatene på innsiden av testcellen. En COMSOL-modell ble brukt med polarisasjonskurver registrert etter hver av testene som grensebetingelser. Denne modellen viste at det største potensielfallet skjedde gjennom det første segmentet, som hadde det minste tverrsnittsarealet som sjøvannet kunne passere gjennom, som også hadde den høyeste motstanden. Modellen viste også lignende strømtetthet som ble målt under testingen og lignende elektrodepotensialer inne i testcellen. Den tredje testen var et galvanisk par mellom SS og NAB. Testen viser det galvaniske parets oppførsel, og måler den strømproduksjonen fra det uedel metallet (NAB), og strømforbruket av det edlere metallet (SS). Over en periode ble det utviklet korrosjonsprodukter på overflaten av NAB. Disse korrosjonsproduktene har ikke blitt undersøkt, men sammenlignet med lignende resultater i litteraturen. Forutsetningen er at ved høyere vannhastigheter vil disse korrosjonsproduktene bli fjernet, og effekten av galvanisk korrosjon vil reduseres.

TABLE OF CONTENTS

LIST OF TABLES

LIST OF FIGURES

Nomenclature

Abbreviations and Symbols

Ag/AgCl	Silver/Silver chloride Electrode
BCC	Body-Centered Cubic
CE	Counter Electrode
CP	Cathodic Protection
FCC	Face-Centered Cubic
ICCP	Impressed Current Cathodic Protection
ISO	International Organization for Standardization
MTP	Department of Mechanical and Industrial Engineering
NAB	Nickel-Aluminium bronze
NTNU	Norwegian University of Science and Technology
OCP	Open Circuit Potential
ppmw	parts per million weighted
PMM	Permanent Magnet Motor
PREN	Pitting Resistant Equivalent Number
RE	Reference Electrode
RDT	Rim Driven Thruster
SA	Sacrificial Anode
SHE	Standard Hydrogen Electrode
SS	Stainless Steel
WE	Working Electrode

I_{corr}	Corrosion Current
$i_{a/c}$	Anodic/Cathodic Current Density
E_{corr}	Corrosion Potential
ΔE	Potential Drop
ρ	Electrolyte Resistivity
R	Resistance

CHAPTER 1

INTRODUCTION

This chapter is an introduction to the outline of this thesis. First a quick description of the background for this thesis in Section 1.1, then a problem description for the thesis, and finally a thesis outline.

1.1 Background

The background for this thesis is the cathodic protection (CP) of an industrial ship propeller based on permanent magnet motor (PMM) technology (7). The propeller in focus consists of Nickel Aluminium Bronze (NAB) and AISI 316L Stainless Steel (SS) parts in mechanical contact. This may lead to galvanic corrosion as the propeller is completely immersed in seawater. To avoid galvanic corrosion, it's possible to either coat the exposed noble metal surfaces or protect the propeller with CP. CP is a well-known method to avoid corrosion and enhance the lifetime of submerged metal. However, most applications of CP are of static structures, with large surface areas that are immobile over its entire lifetime. A propeller will either rotate at a high speed (peripheral velocity of about 30 $\frac{m}{s}$ is normal for the propeller in focus) or be at standstill when the ship is at quay. For the propeller in focus, the exposed metal surfaces

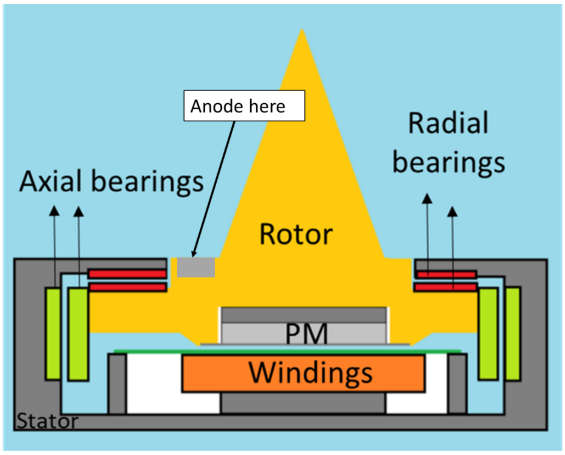

Figure 1.1: Cross section of a PMM with the implementation of a sacrificial anode (2).

are also situated in a confined space due to the design of a PMM. The rotating part, the rotor, is a ring with propeller blades fixed in the rim, concentrically placed inside a larger ring, the stator. Between the rotor and stator, there is a narrow gap, to reduce power loss between the magnets. This gap is filled with seawater, and CP may have problems to protect the exposed metal in this region due to potential drop through the gap between rotor and stator. Figure 1.1 illustrates the cross-section of the PMM, including a sacrificial anode(SA). A project was carried out prior to this master thesis where a test cell was created to be used for further testing. This test cell was created to have an identical shape as the rotor and part of the axial bearings, but was made of acrylic and plexiglas. Samples of each material were then cut out and prepared, and were then placed on the acrylic structure to represent the metal. Figure 1.2 shows the finished test cell after the samples and wires were connected.

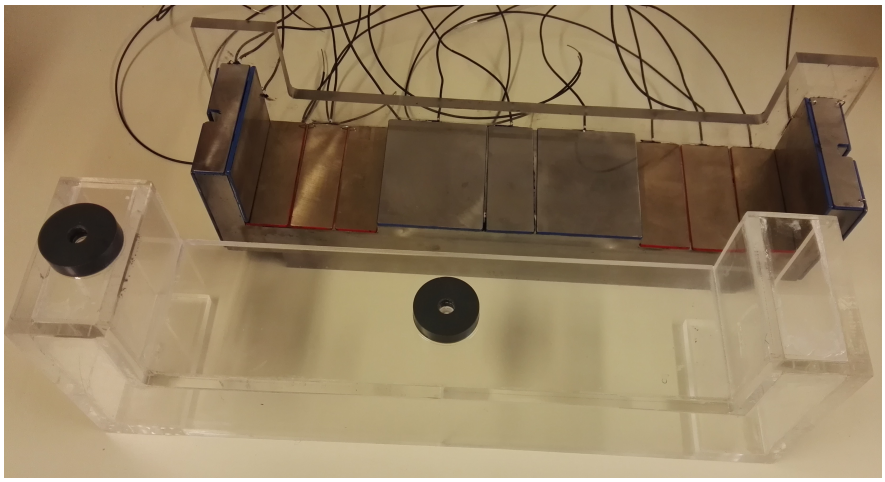

Figure 1.2: Finished test cell with samples from preliminary project.

1.2 Problem Description

The main objective of this thesis was to document how well NAB on the outer diameter of the rotor can be protected with anodes placed on the inner diameter of the propeller, with special regard to the potential drop through the electrolyte. For this thesis, there are three main objectives:

- How well can CP protect corrosion inside the structure?
- How will galvanic corrosion affect the NAB samples?
- How well can the corrosion physics be modeled in COMSOL Multiphysics (8), and how reliable are these results?

1.3 Thesis Structure

The aim of this thesis is to experimentally test protection of the samples with and without CP and water flow. The results from these experimental tests will then be used in a computer program called COMSOL Multiphysics (8) which has the ability to calculate the potential distribution and current density for the metal surfaces in the structure geometry. The results will then be compared and discussed. The outline will begin with theoretical research for theory relevant to these tests, followed by three experimental tests including testing with:

- Cathodic protection in stagnant conditions.
- Cathodic protection with water flow.
- Galvanic couple with water flow.

These experimental tests will then be modeled in COMSOL using experimental results as boundary conditions. The results from these tests will then be displayed, and subsequently discussed. Finally a conclusion and a list of future work.

CHAPTER 2

THEORY

2.1 Introduction

The theory used in this master thesis will involve the topics within electrochemistry, as well as theory about the different materials used. Since this thesis is about galvanic corrosion between SS and NAB and CP of these, they will be included in this chapter. It will also include theory about a potential drop in the electrolyte, and equations that describes the mathematical way to calculate the potential drop through the test cell. This chapter will also include theory about electrode kinetics.

Cathodic protection through geometrically confined spaces relies on the protection current from the sacrificial anode (SA) to reach the corroding surface. Krupa et. al. (9) investigated a NAB ballast hull used on Navy vessels. Their approach to evaluate the efficiency of CP on internal components through confined space was to use both boundary element method and physical testing to understand the effects of current distribution. Their hypothesis was that with a small cross-sectional area for the water to flow would lead to a high fluid resistance, which would lead to a high potential drop through the confined space. This potential drop would then be so large that the material at the other end of the confined space would not be protected. The fundamentals of CP is an external supply of electrons to reduce the anodic reaction of the protected metal. These electrons can be supplied by sacrificial anodes or an external power supply. However, to be able to properly protect the surface, a current density requirement must be met. This requirement changes based on surrounding environment, and as in this thesis, water flow is added. Sawyer et. al. (10) investigated the current density requirement for cathodic protection, and wrote that; ”For any given potential,

the current requirement also increases with the increased speed of water relative to the surface.". In their experiment with circulating water, they discovered that for steel in 15 C^o seawater, the current density increased rapidly from near 0 $\frac{cm}{sec}$ to 5 $\frac{cm}{sec}$. Then the increase leveled out to a more linear increase in current density relative to water speed. During CP, calcareous deposits develop on the surface of SS. This deposit creates a barrier between the steel surface and the electrolyte (seawater). The current requirement in the North Sea is in the region of 200 $\frac{mA}{m^2}$ (3) after initial exposure. However, this requirement will decrease, and the cathode efficncy will decrease over the first couple of days due to the formation of calcareous deposits. Upon immersion in natural seawater, biofilm formation becomes a concern. The biofilm produces enzymes on the metal surface which catalyze the oxygen reduction reaction which increase the cathode efficiency (7).

2.2 Electrochemistry

The basics of electrochemistry are the charge transfer reactions, also called the electrode reactions. The electrode reactions are two reactions, the oxidation reaction and the reduction reaction. The oxidation reaction occurs on the anode. It dissolves the metal M and transfers the metal in form of ions (M^{n+}) into the electrolyte. On the opposite side, there is a reduction reaction which occurs on the cathode. In natural environments, the most common reduction reaction is the reduction of oxygen. The process between the anode and the cathode create an electric circuit where the electrons are released in the anode and are transported through the metal to the cathode where it's used in the oxidation reaction (4). The oxidation reaction is dissolving according to Equation 2.1.

$$\text{Oxidation Reaction} : M \Rightarrow M^{n+} + ne^- \tag{2.1}$$

And the dissolution of oxygen in the reduction reaction in Equation 2.2:

$$\text{Reduction Reaction} : O_2 + 2H_2O + 4e^- \Rightarrow 4OH^- \tag{2.2}$$

The anodic and cathodic polarization of a metal(M) can be seen in Figure 2.1.

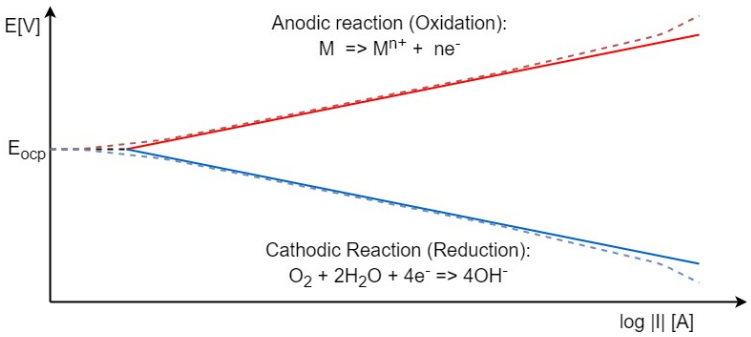

Figure 2.1: Anodic and cathodic reaction of a metal.

In an electrochemical cell, there is an anode, where the oxidation reaction occurs, and a cathode, where the reduction reaction occurs. Both of the electrode reactions in the electrochemical cell can be associated with an electrode potential. Placing a high resistance voltmeter in the circuit between the anode and the cathode, the cell potential can be measured. The cell potential is the potential difference between the cathode and the anode, see Equation 2.3

$$E_{cell} = E_{cathode} - E_{anode} \tag{2.3}$$

To accurately measure the cell potential, a reference electrode(RE) is necessary. The reference electrode is a known reference to measure against, and two commonly used REs are the standard hydrogen electrode (SHE) and the silver/silver chloride (Ag/AgCl) electrode. The Ag/AgCl electrode is mainly used for seawater applications (11). When using a reference electrode, the RE is set as one of the half-cell reactions, while the other half-cell reaction is the electrode potential on the metal being measured. This metal is no longer an anode or a cathode but is referenced as the working electrode (WE).

2.3 Galvanic Corrosion

Galvanic corrosion is a common and dangerous type of corrosion (11). It occurs when two different metals come in metallic contact in the presence of a corrosive environment. When two metals are in contact with an electrolyte, the electric circuit between these metals is closed. The net flow of current will flow through the two metals and the electrically leading environment. This closed circuit functions like a power generating battery, at open circuit potential (OCP), both metals will equilibrate at the respective corrosion potential. Equation 2.4 shows the relationship between the corrosion potentials of the noble and active metal.

$$\Delta U = E_{corr(M)} - E_{corr(N)} > 0 \tag{2.4}$$

Where ΔU is potential difference, $E_{corr(M)}$ describes the corrosion potential of metal M and $E_{corr(N)}$ describes the corrosion potential of metal N. When the circuit is closed, $\Delta U = 0$ and the two metals stabilize at the same potential. The closed circuit potential can be described like this:

$$E_M = E_N = E_{couple} \tag{2.5}$$

This galvanic relationship is also described in Figure 2.2.

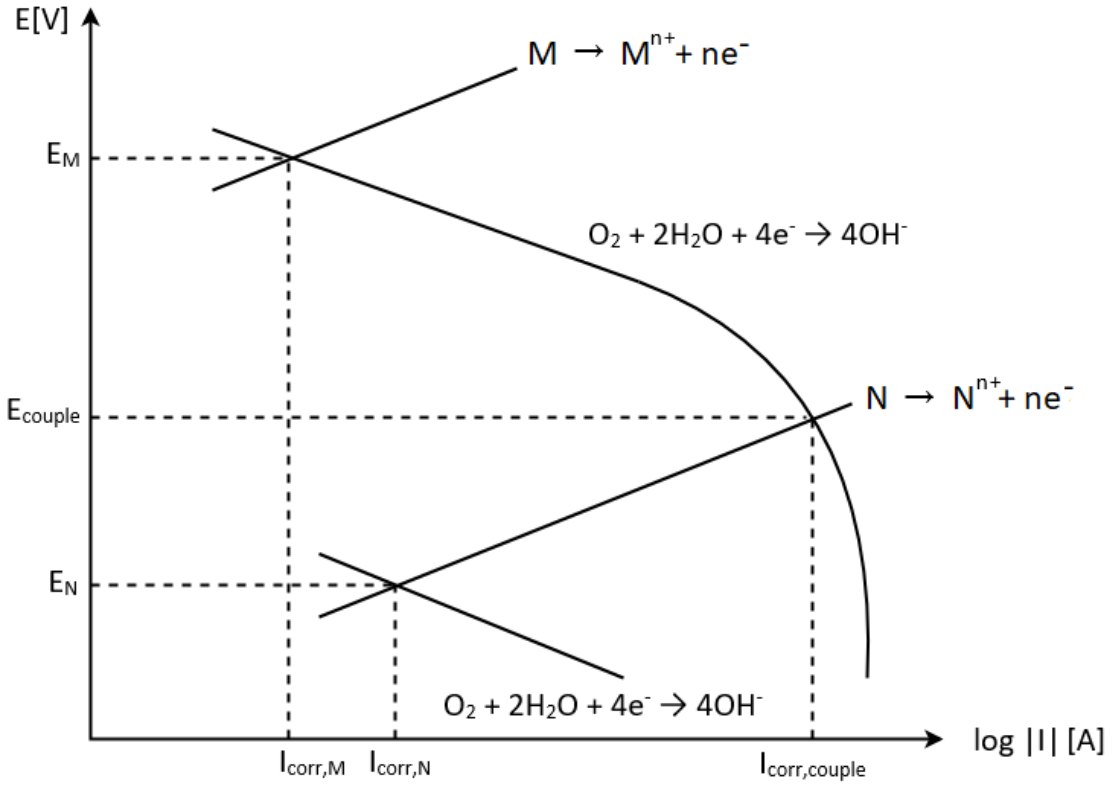

Figure 2.2: Graphical illustration of a galvanic couple between two metals with different nobility. E_{couple} describes the combined corrosion potential, and $I_{corr,couple}$ describes the combined corrosion current (3).

The result from this relationship is a net positive current that flows from metal N to metal M with the assumption that M is nobler than N. This generation occurs because of an increased oxidation of the active metal relative to its oxidation rate under OCP. The active metal will dissolve at a higher rate when in contact with the noble metal than if it was under open circuit conditions. This will also lead to a reduced dissolution rate on the noble metal (11). The dissolution of the active metal is called galvanic corrosion, while the reduced dissolution rate on the noble metal is actively used to reduce dissolution rate and is the principle behind cathodic protection. In a galvanic couple, the surface area of each metal affects the impact of galvanic corrosion. The surface area ratio between

the anodic surface area and the cathodic surface area is an important parameter to consider when using sacrificial anodes in CP. When considering charge transfer inside an electrochemical cell, the number of electrons produced on the anode must be identical to the number of electrons consumed on the cathode. This relationship is expressed in Equation 2.6:

$$\Sigma I_a = \Sigma I_c \Rightarrow \Sigma i_a A_a = \Sigma i_c A_c \tag{2.6}$$

Where I is the current [A], i is the current density [Ampere per surface area] and A is the surface area. In a galvanic cell, the anodic reaction on the cathode and the cathodic reaction on the anode has to be added to the Equation. However, with the assumption that the anodic reaction on the cathode and the cathodic reaction on the anode are negligible (very small values), Equation 2.6 can be further derived to Equation 2.7:

$$i_a A_a = i_c A_c \Rightarrow i_a = i_c \frac{A_c}{A_a} \tag{2.7}$$

The relationship to the right of the arrow in Equation 2.7 demonstrates the surface area impact of galvanic corrosion. It is important to avoid large surface area ratios where the cathodic surface area is much larger than the anodic surface area. This is because the anodic current density is proportional to the surface area ratio, and would lead to a more aggressive galvanic corrosion. Figure 2.2 illustrates the galvanic connection between noble metal M and active metal N. Both these metals are tested in the same corrosive environment and shows OCP relative to the galvanic series (12). The noble metal has a higher potential than the active metal. When these two metals are in metallic connection in the same corrosive environment, the combined potential will stabilize at a common galvanic potential. The combined potential will decrease for the noble metal, and increase for the active metal. This will also increase and decrease corrosion potential in the respective metals (11). For the noble metal, this reduction in potential will also reduce corrosion current, which will reduce the corrosion rate. With the occurrence of an ohmic resistance against the flow of current, the potentials of the anode and the cathode in the solution is not equal (11). This difference in potential between the anode and the cathode is given by:

$$E_M - E_N = I_{net} * R \tag{2.8}$$

Where E_M is a noble metal, and E_N is an active metal in a galvanic connection, I_{net} is the measured flow between the anode and cathode in the galvanic connection, and R is the ohmic resistance

between them. The ohmic resistance in a galvanic connection is in the electrolyte, which can be a liquid solution or the dirt in the ground. The ohmic resistance varies with which electrolyte it's in, and can be calculated. The ohmic resistance in the electrolyte can be described by Equation 2.9:

$$R = \rho \cdot \frac{L}{A} \tag{2.9}$$

Where ρ is the resistivity of the electrolyte [ohm $\cdot$ m], A is the cross-sectional area and L is the length of the materials. The conductivity of the electrolyte and the geometry of the system both take part in deciding the potential drop of the system. A low cross-sectional area and a long distance between the anode and the cathode will help create a high potential drop. Figure 2.3 illustrates how a potential drop between the metals will reduce the galvanic corrosion.

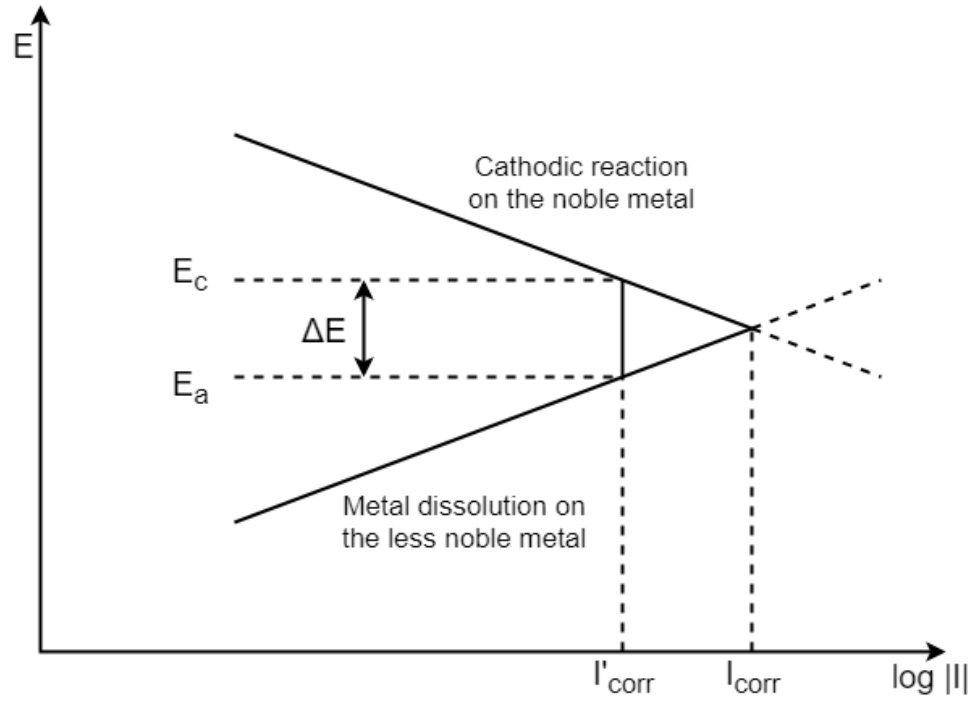

Figure 2.3: Illustration of potential drop in the electrolyte where I_{corr} is the corrosion current without a potential drop, I'_{corr} is the corrosion current with a potential drop, E_c is the cathode potential on the entire noble metal surface and E_a is the anodic potential on the entire unnoble metal surface (4).

2.3.1 Calculation of potential drop

While it is experimentally possible to measure the difference in potential between the sacrificial anode and a metal sample, it is also theoretically possible to calculate the potential drop (ΔE). This can be done by calculating each segment individually. Each segment includes the metallic surface area of the samples in the segment and the cross-section of the water. It is assumed that the geometrically confined structure is laid out and treated as a pipe as shown in Figure 2.4.

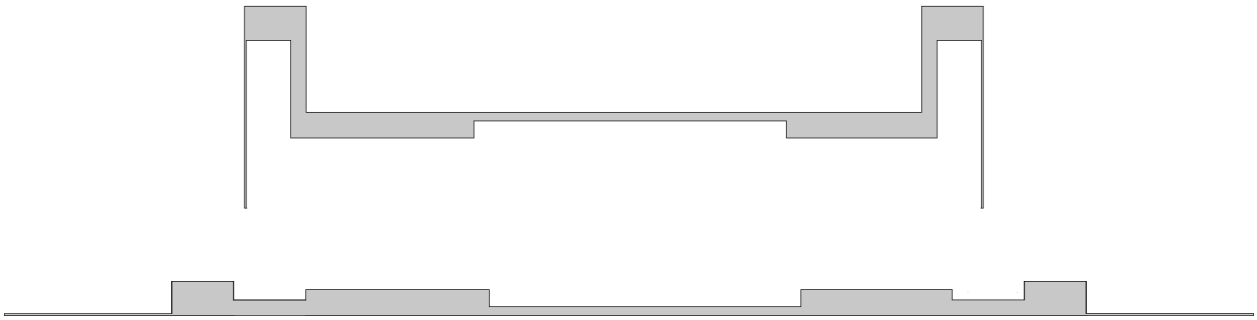

Figure 2.4: Front side view of the electrolyte, and the electrolyte laid out to illustrate the assumption used in the calculation. The assumption that the electrode surface is represented by the straight bottom line, with changing volumes of electrolyte.

In Figure 2.4, the bottom edge is the metal samples as can be further illustrated in Figure 2.5.

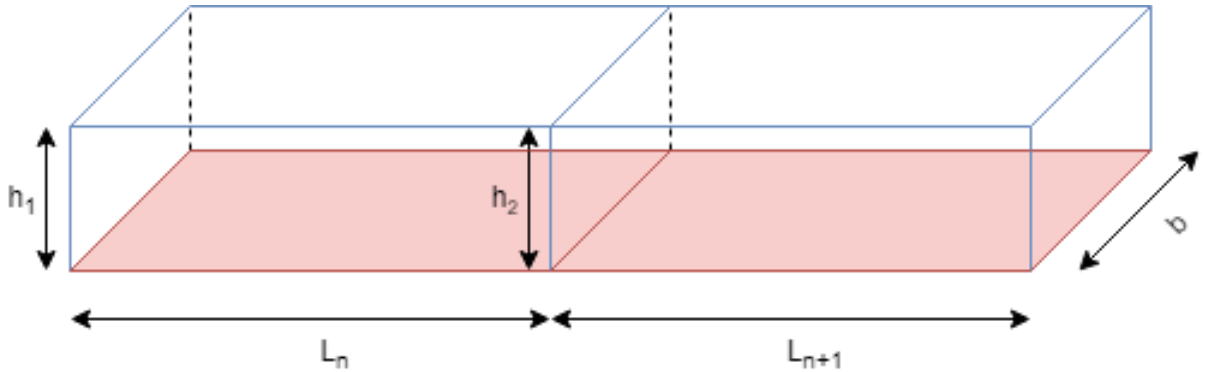

Figure 2.5: Representative figure to show the electrode surface boundary, with the cross section above. This cross section varies with changing segment.

The test cell has two water inlets, one on each side of Figure 2.4. The potential drop is theoretically decided based on surface area ratio, electrolyte conductivity, and system geometry. Based on these conditions in the test cell, the hypothesis is that the largest potential drop, or the most positive

potential, will be in the middle of the geometry. Because of this hypothesis, the calculation of the potential drop will only be carried out on one half of the geometrical confined structure.

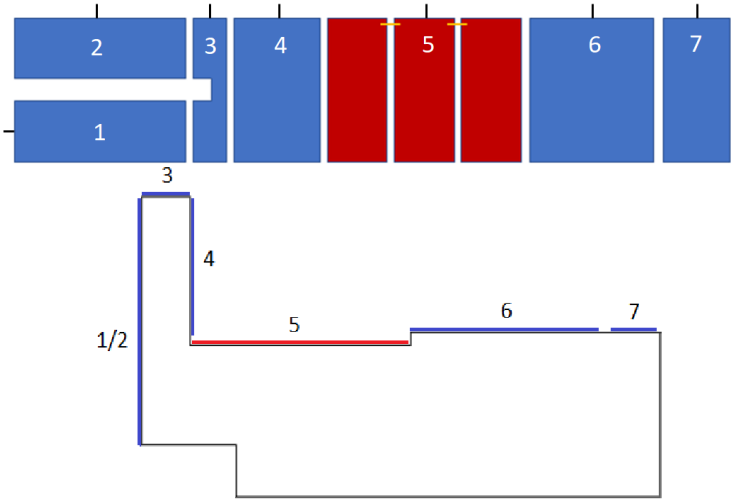

Figure 2.6: Representation of the setup and samples used in the calculation of potential drop.

This is a presentation of an analytical way to calculate potential drop. It is an approximation to a real value, and it disregards several key aspects of potential drop through a geometry. When using Equation 2.10 and 2.11, the assumption is made that the potential on a sample is the same for the entire surface. The calculation of the potential drop through the geometrically confined structure is done using these two equations:

$$\Delta E_N = \frac{\rho}{h_N \cdot w}\left[I_N \cdot L_N - \frac{1}{2}\cdot i_N \cdot w \cdot L_N^2\right], N = 1 \text{ and } 2,\ 3,\ 4,\ 5,\ 6 \tag{2.10}$$

$$\Delta E_7 = \frac{\rho \cdot i_7}{2 \cdot h_7} \cdot L_7^2 \tag{2.11}$$

Where ρ is the electrical conductivity of the electrolyte, h_N is the height of the electrolyte in the segment, w is the width of the test cell, I_N is the current reaching the sample, L_N is the length of the segment and i_N current density consumed by the segment. The derivation for these formulas can be found in Appendix A. The geometries in this calculation are for the electrolyte, the width is constant for the test cell, but the height and the width varies. This is illustrated in Figure 2.4 and 2.5. The anode is placed beneath the test cell, and the water inlet is just below sample 1/2. The electrolyte path runs past sample 1/2 on the left, over the edge past sample 3. Then runs down past sample 4, and runs horizontally past sample 5, 6 and 7. The current (I_N) and current density (i_N) are taken from the experimental test in natural seawater. The current is measured by placing a

known resistance between the sacrificial anode and the metal sample, and the potential drop (ΔE) is measured. The current from each sample can then be calculated. The total current that is consumed by the samples (both SS and NAB samples) are then summed up, and this is the total current from the anode and is called I_N. This means that the sacrificial anode delivers a current I_N to the water inlet below sample 1/2. The current is then consumed by sample 1 and 2, and the current provided to sample 3 would then be $I_N - I_{1/2}$. The total amount of current will then be completely consumed when passing sample 7. The calculated potential drop will be provided in Chapter 5.

2.4 Cathodic Protection

The basics of cathodic protection (CP) is to protect a steel structure from corroding by applying a current. This current can be produced in two ways, either by applying a direct current to the galvanic connection or by installing a sacrificial anode (13). The CP is active in a presence of a cathode, an anode, electrical connection, and electrolyte. When steel is exposed to seawater, these reactions will occur:

$$\text{Anodic Reaction: } Fe \Rightarrow Fe^{2+} + 2e^{-} \tag{2.12}$$

$$\text{Cathodic Reaction: } O_2 + 2H_2O + 4e^{-} \Rightarrow OH^{-} \tag{2.13}$$

The anodic reaction (Equation 2.12) is the consumption of metal and release of electrons, while the cathodic reaction (Equation 2.13) represents the consumption of electrons and dissolution of hydroxyl ions (OH^{-}). With these definitions, it's possible to envision what might happen if either reaction would increase. If electrons were removed from the metal surface, the anodic reaction would increase to make up for the lost electrons and would lead to an increase in metal consumption. This would also slow down the cathodic because of the reduction of available electrons. However, if electrons were introduced to the metal surface, the cathodic reaction would increase and the anodic reaction would slow down, which again would slow down the metal consumption. For a single piece of metal without any external supply of electrons, both the anodic and cathodic reactions will occur simultaneously. The anodic reaction will deposit electrons into the electrolyte which the cathodic reaction will then consume. This sequence will continue until the metal has reached reversible potential. This is further illustrated in Figure 2.7a. With cathodic protection either with impressed current cathodic protection (ICCP) or sacrificial anodes, an external current is introduced to the metal surface to eliminate the electrons provided by the anodic reaction. This then removes the metal dissolution, and protects the surface (3), see figure 2.7b.

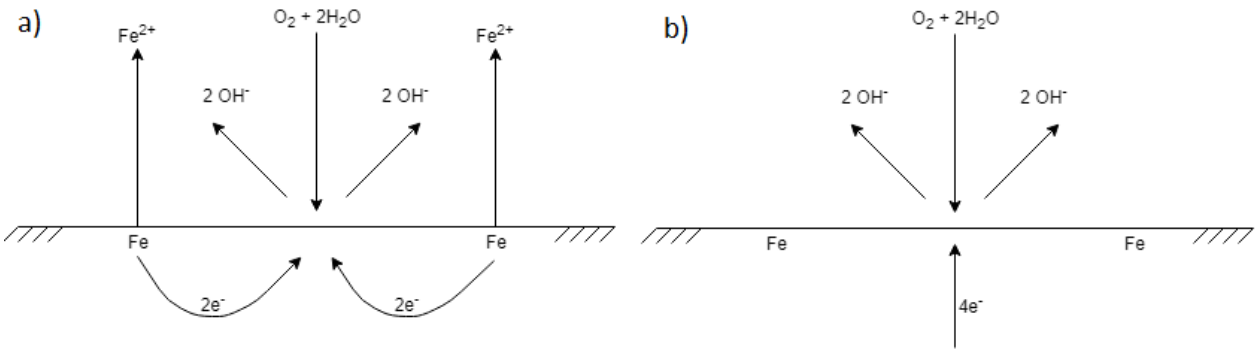

Figure 2.7: Figure a) illustrates a freely exposed metal in a corrosive environment. The metal then works as the anode and as the cathode, where the electrons provided in the anodic reaction provides electrons for the cathodic reaction. Figure b) illustrates a metal in a corrosive environment where the electrons are externally provided, to avoid the anodic reaction (3).

A protection potential for sufficient CP can be achieved, and standards are made for potential criteria for various metals and alloys in seawater (1). For austenitic steels containing chromium and/or molybdenum, a minimum negative protection potential is set to -0,3V vs. Ag/AgCl. While for copper alloys with aluminium a minimum protection potential is set to -0,45V to -0,60V vs. Ag/AgCl. The protection potential for a given metal can be illustrated in a polarization diagram, see Figure 2.8.

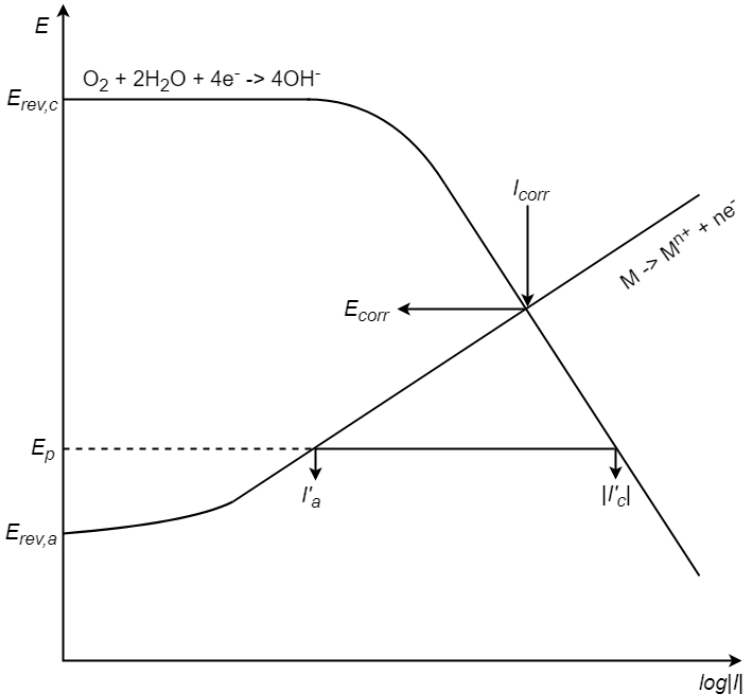

Figure 2.8: Polarization diagram representing corrosion and cathodic protection (3).

Both the anodic and cathodic reactions are at equilibrium at E_{corr}. Then the corrosion current is given by I_{corr}. Here, I_{corr} is a representation of the cathodic and anodic reactions rate at the given potential. At this potential, the rate of electron release is identical to the electron consumption. Additionally, there is no net current flow, but there is metal consumption. In Figure 2.8, I_{corr} represents the metal dissolution rate at a given potential. To reduce the dissolution rate, and protect the metal from corroding, the potential has to decrease. Without any external assistance, the anodic and cathodic reactions will drift towards equilibrium at E_{corr}. To protect the metal from metal dissolution, the potential has to be reduced to E_p. However, at this potential, the electrons provided by the anodic reaction at I'_a are not sufficient to supply the consumption of electrons in the cathodic reaction at I'_c. This means that to reduce the potential to a protection potential, an external supply of electrons of I'_c-I'_a must be provided to reduce the metal dissolution rate from I_{corr} to I'_a. An ISO standard is created to set a minimum negative protection potential of commonly used materials in seawater. Table 2.1 shows the different protection potentials for the two metals used in this Thesis. These protection potentials will be the target for CP.

Table 2.1: ISO standard for CP of commonly used alloys in seawater (1).

Material	**Minimum Negative Potential [V vs. Ag/AgCl/Seawater]**
Austenitic steels containing chromium and/or molybdenum	
(PREN $\geq$ 40)	-0,5
(PREN <40)	-0,3
Copper alloys	
without aluminium	-0,45 to -0,60
with aluminium	-0,45 to -0,60

Pitting Resistance Equialent Number(PREN) is used as an indication of the resistance of a corrosion alloy to pitting in the presence of water, chlorides and oxygen (1).

2.4.1 Calcareous Deposits

An important factor affecting charge transfer at metal surface is calcareous deposits or calcareous scale. A calcareous scale is formed by decomposition of seawater during cathodic protection. The formation of calcareous scale occurs because of the production of hydroxyl(OH^-) ions dur-

ing oxygen reduction which increases the pH at the metal surface. See Equation 2.13. With the presence of CO_2 in seawater, carbonate(CO_3^{2-}) and bicarbonate(HCO_3^-) are present, and are in a pH-dependent equilibrium with each other (3)(11)(14)(15):

$$CO_2 + H_2O = H_2CO_3 \tag{2.14}$$

$$H_2CO_3 \rightleftharpoons H^+ + HCO_3^- \tag{2.15}$$

$$HCO_3^- \rightleftharpoons H^+ + CO_3^{2-} \tag{2.16}$$

Because of the presence of OH^-, the pH at the surface increases. With increased pH, the reactions in equation 2.15 and 2.16 are favored to the right, leading to a higher concentration of carbonate. In seawater, Ca^{2+} and Mg^{2+} occur naturally, and precipitation with Ca^{2+} and Mg^{2+} becomes possible at the metal surface, which leads to (11; 14):

$$Ca^{2+} + CO_3^{2-} \rightarrow CaCO_3(s) \tag{2.17}$$

$$Mg^{2+} + 2OH^- \Rightarrow Mg(OH)_2(s) \tag{2.18}$$

With an increased concentration of carbonate-ion, the equilibrium of calcium carbonate($CaCO_3$) deposition is favored, see Equation 2.17. The increase in carbonate concentration is caused by an increase in pH, which again is caused by the increased OH^- concentration. The $CaCO_3$ is developed as a film on the metal surface and is referred to as a calcareous deposit. This is a secondary effect of cathodic protection. These deposits form a non-conducting insulating film on the surface which works as a barrier against oxygen diffusion which then reduces the current density requirement for CP.

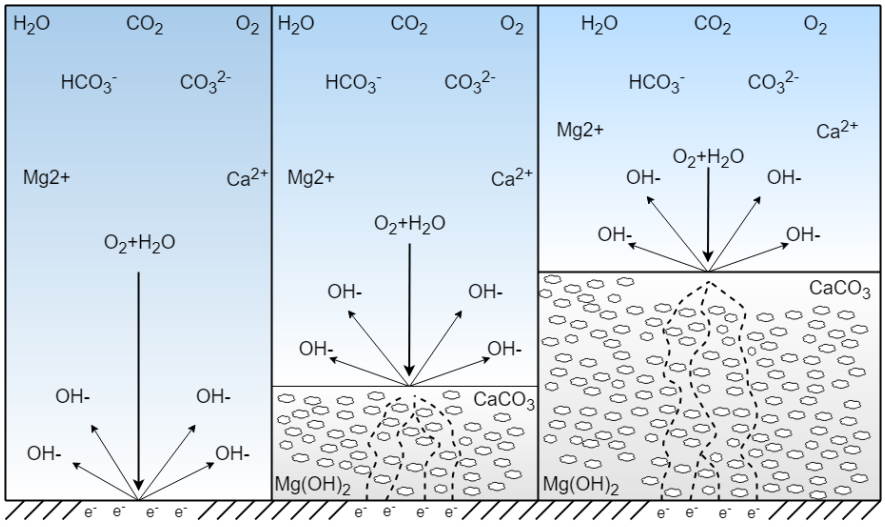

Figure 2.9: Illustration of the barrier provided by calcareous deposits. Illustration is adapted from (5).

2.5 Nickel Aluminium Bronze

Nickel-aluminium bronzes are alloys containing 9-12% aluminium and up to 6% of iron and 6% of nickel. The most common alloys contain about 3-6 % each of iron and nickel and have been fully investigated in their combination of properties. The main component in the Ni-Al bronze alloys is copper. The most common alloy compositions contain approximately 80 wt% Cu and supplemented with various alloys to obtain the correct mechanical properties. Al is primarily responsible for the increase in tensile properties, in combination with Nickel. The phase-diagram for Cu-Al is further illustrated in Figure 2.10.

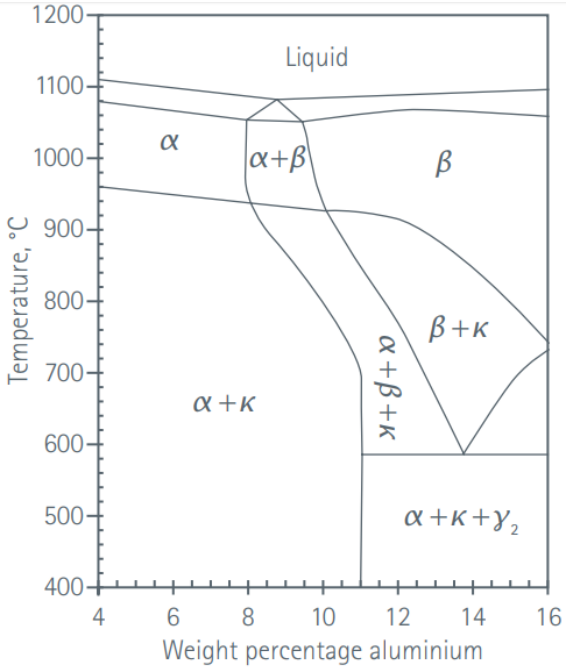

Figure 2.10: Cu-Al-Ni-Fe phase diagram at 5 wt% each of nickel and iron (6).

The phase diagram in Figure 2.10 contains several phases including the α, β and the κ phases. The α phase is a copper-rich stable solution with a face-centered cubic(fcc)-structure. It provides ductility to the alloy, while other phases increase tensile strength and hardness. The β phase requires high temperature, and is an intermediate solid solution with a body-centered cubic(bcc) structure, and contains a high amount of aluminium. During cooling of the alloy, most β phase is transformed into α, however, if the cooling rate is too high, retained β phase can occur at room temperature. It is an unwanted phase and is often heat treated out of the alloy. The κ particles are intermetallic compounds that with one exception either forms Fe_3Al or $NiAl$. The one exception is the κ_I which either forms Fe_3Al or $FeAl$(6). This is a very brief description of the phase diagram, for further reading and understanding, please read H. Meigh, "Cast and Wrought Aluminium Bronzes" chapter 13 (6).

Nickel-aluminium bronze has a high resistance to seawater corrosion due to the surface protection of its oxide film (6). Schüssler (16) researched the protective layer formation and passivation mechanism of Ni-Al bronze in synthetic and natural seawater. He found a formation of an 800nm thick layer consisting of Mg, Al, Cu and Fe oxides when exposing Ni-Al bronze at OCP in synthetic seawater, with the inner layer enriched with Al and the outer layer enriched with Cu. Schüssler

found that this layer would reduce the corrosion current by a factor of 20-30. This was achieved by anodic passivation due to the formation of Al-oxide which hampered the ionic transport across the corrosion product (16). It also formed of cuprous oxide in the outer layer of the protective film, which reduced the charge transfer of the oxygen reduction and decreased the cathodic reaction rate (16).

Table 2.2: Composition of NAB

Element	Cu	Al	Fe	Ni	Cr	Mg	Mn	Pb	Sn	Zn
wt%	80.52	9.44	4.23	5.04	<0.005	<0.01	0.72	<0.01	0.01	0.03

2.6 Stainless Steel

Stainless steels are a family of engineering materials, often chosen for their corrosion and heat resistant properties. Apart from containing iron and carbon, their common denominator is the presence of chromium and nickel.

In addition to chromium and nickel, several other materials are included to strengthen various physical properties. They are all capable of changing the materials properties in some way, which can help address machinability or further improve the corrosion resistance. A general chemical composition for AISI 316L SS can be seen in Table 2.3.

Table 2.3: Composition of UNS S31603 AISI 316L stainless steel.

Element	C	Si	Mn	P	S	Cr	Mo	Ni	Fe
wt%	0.03	0.75	2	0.045	0.03	17	2.5	12	65

The AISI 316L alloy is a common choice when corrosion resistance is of interest. The relatively high percentage of chromium (16-18%) is the foundation for the corrosion resistance. In terms of mechanical properties, chromium also improves hardenability, response to heat treatment and wear resistance. Nickel is an essential alloying element, as the presence of nickel provokes the formation of an austenitic structure. In other words, it increases the temperature span in which austinite can be formed. For this reason, nickel is often termed an austenite stabilizer (17). In addition to this, it increases the hardness penetration and the high-temperature tensile strength.

After SS is exposed to natural seawater, the chromium forms a thin, stable, regenerative passive film on the surface of the chromium-rich oxide (18). This oxide film is a thin protective layer on the surface of the metal that reduces reactions on the metal surface. These films are regenerative, which

means if the film is damaged, the chromium in the steel reforms the protective layer. Biofilm formation occurs on the surface shortly after immersion in natural seawater. The biofilm on the metal surface increases the cathode efficiency of SS and initiates an increase of the corrosion potential. Biofilm formation is further explained in the next chapter.

2.7 Biofilm Formation

Biofilm is a concern in natural seawater and can affect both SS and NAB. The effect of biofilm on SS is well documented. The biofilm activity produces enzymes which catalyze the oxygen reduction reaction (2). The effect of biofilm on SS is initially delayed after initial exposure by 40-120 hours before a sharp increase in potential from below -100mV to +250mV vs. Ag/AgCl, and an increase to +380mV vs. Ag/AgCl during a 10-20 day period. Biofilm formation on metal surfaces takes time to develop, however, the effect is an increase in cathodic current density and by Faraday's law an increase in corrosion rate (11). Biofilm is known to be limited on NAB because of the toxicity copper ions release. This toxicity diminishes with the dissolution of copper, however, the effect is not registered until several months after exposure.

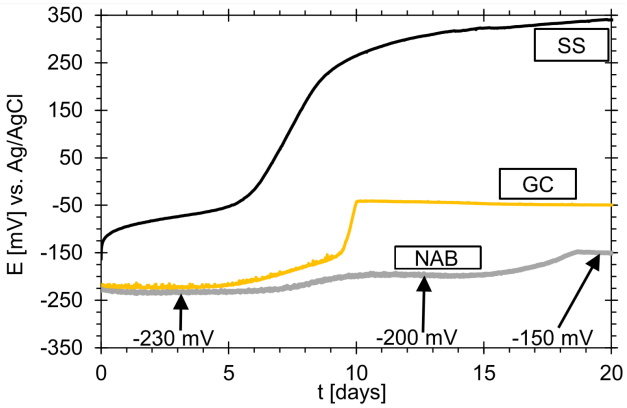

Figure 2.11: OCP of freely exposed SS and SS, and of the galavnic coupling potential of SS and NAB (2).

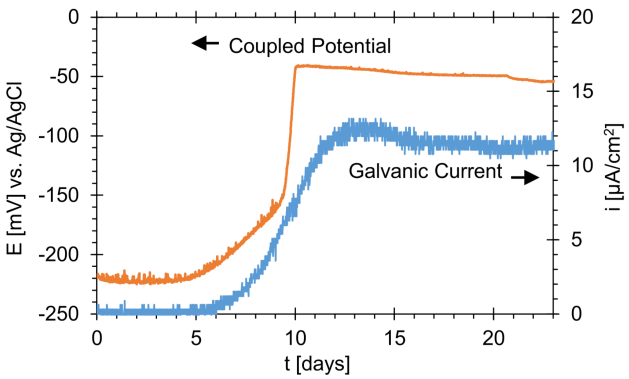

Figure 2.12: The galvanic potential and the galvanic current of NAB and SS coupled together (2)

Krogstad and Johnsen (2) investigated the cathodic behavior of polarized SS, both in galvanic contact with NAB, and cathodic polarization of samples of SS to the same potential steps of the galvanic couple during 25 days of exposure. They also investigated the OCP of freely exposed NAB, SS and the OCP of the galvanic couple between them. The result of these tests can be seen in Figure 2.11. Figure 2.12 shows the galvanic couples potential and the galvanic current density. Freely exposed SS has a linear

increase the first six days, before a sharp increase in OCP. The sharp increase for SS is attributed to the formation of biofilm on the metal surface (2). After the sharp increase, the OCP gradually increases at a more moderate speed beyond 0,3V vs. Ag/AgCl. Freely exposed NAB goes through three steps of ennoblement during the first weeks of exposure. The first step occurs between five to ten days and is an increase in OCP from -230 to -200mV vs. Ag/AgCl and is hypothesized to correlate with an increase in cathodic reaction rate due to biofilm formation (2). The second step occurs between 15 to 20 days and is an increase from -200 to -150mV vs. Ag/AgCl. This step is caused by the growth of protective films that decrease the anodic and cathodic reaction rates. For the galvanic couple between NAB and SS, the OCP is initially similar to the OCP of freely exposed NAB, before an increase in both OCP and current density after six to ten days. This increase in galvanic current is attributed to the biofilm formation.

CHAPTER 3

COMSOL MULTIPHYSICS®

3.1 Introduction

COMSOL Multiphysics (8) is a general-purpose platform software for modeling engineering applications. Within COMSOL there are several different modules; electromagnetics, structural mechanics, fluid flow and chemical engineering are among a few. There are many other topics which COMSOL can model, however, for this thesis the corrosion and electrochemistry module is the most important (19). The objective for the use of COMSOL Multiphysics is to construct a replica of the test cell model that is used for experiments in Sealab, and use the multiphysics aspect of COMSOL to compare the results. The idea is to create a close to identical replica in terms of model and data results and to eventually be able to run further tests only using this software.

The geometrical model was initially created to replicate the test cell used for the experiments. However, when using the corrosion module, the electrolyte is the important factor. This is because COMSOL calculates the current flow in the electrolyte, and current consumption by the electrodes to measure the potential drop through the geometry.

3.2 COMSOL Model

The initial approach to creating the COMSOL model was to create an identical representation to the real model. By doing this, the model would include subsurface material. When considering corrosion of metals, it's always the surface area which is of interest, and when calculating potential drop through an electrolyte, it's the surface area which is considered. Therefore, using an identical representation of the realistic model would include unnecessary material to calculate, and would require unnecessary computing power. The modeled electrolyte can be seen in Figure 3.1.

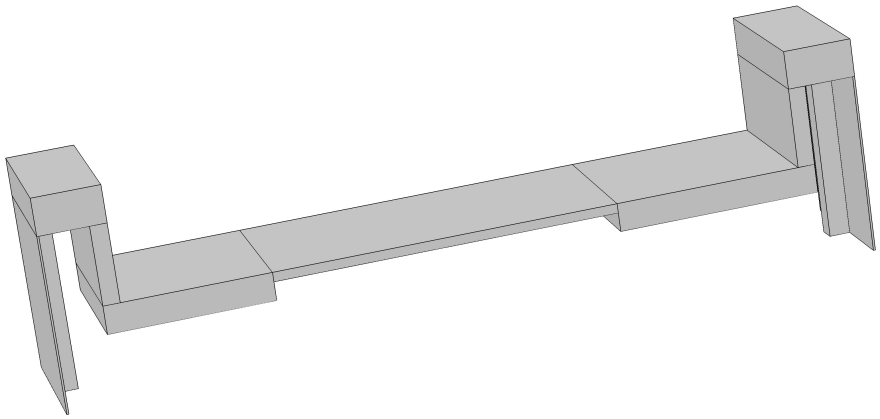

Figure 3.1: Model of the electrolyte inside the test cell.

Since there is confined geometrical space for the electrolyte to pass through, it's possible to model the complete volume of electrolyte inside the test cell. After the electrolyte is modeled, COMSOL has a function to select boundary conditions of the electrolyte, and determine a material surface. This is then done for SS, NAB and for the aluminium anode. Every boundary that has not been given a specific material surface, are isolated surfaces and will not conduct any electrochemical reactions. In this model, the anode is not added in the same identical way as in the experiment. Instead, the surface boundary on each side of the test cell where the inlet of water is in the realistic model is set to be aluminium. This is not an unrealistic assumption, as during the first experiment a reference electrode was used to measure the corrosion potential of the aluminium anode in the testing tub. The potential of the anode was identical when measured right next to the anode as the potential measured close to the water inlet. The aluminium anode was placed approximately 15-20 cm away from the water inlet. Figure 3.2 illustrates the electrolyte model with the material boundary surfaces selected.

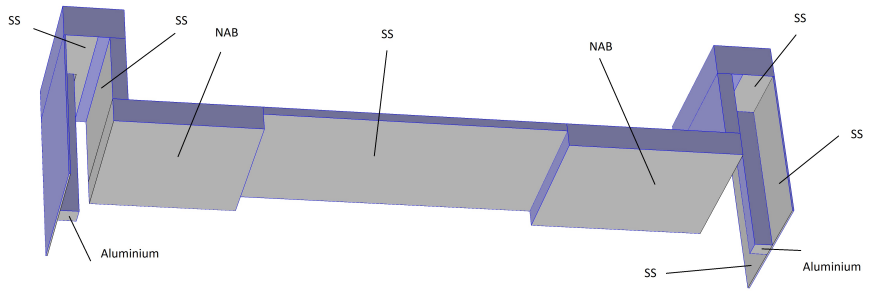

Figure 3.2: Model of the electrolyte inside the test cell with material surfaces added. The blue represents the electrolyte, while the grey represents the boundary surfaces.

COMSOL has a function in the corrosion module for use of primary and secondary current distribution. Primary current distribution only accounts for losses in the electrolyte, while secondary current distribution also accounts for the effect of the electrode kinetics. The main difference between the two is the electrochemical reaction between the electrolyte and an electrode. For this model, secondary current distribution is selected. The function for secondary current distribution in COMSOL gives you the ability to add boundary conditions to the materials such as polarization curves. Polarization curves are added as electrode kinetics for each metal and gives the tests a more realistic result. Actual boundary conditions were measured in the tests and used in the modeling.

CHAPTER 4

EXPERIMENTAL WORK

4.1 Introduction

This master thesis is continued work of a preliminary project done during the previous semester. During the preliminary project, a replica Rim Driven Thruster (RDT) was created. The thruster in question is a RDT 800 (20). The number 800 refers to the propeller diameter (21) and the replica is 1:2 the size of the real thruster. In figure 4.1 the finished test cell after production during the preliminary project is displayed.

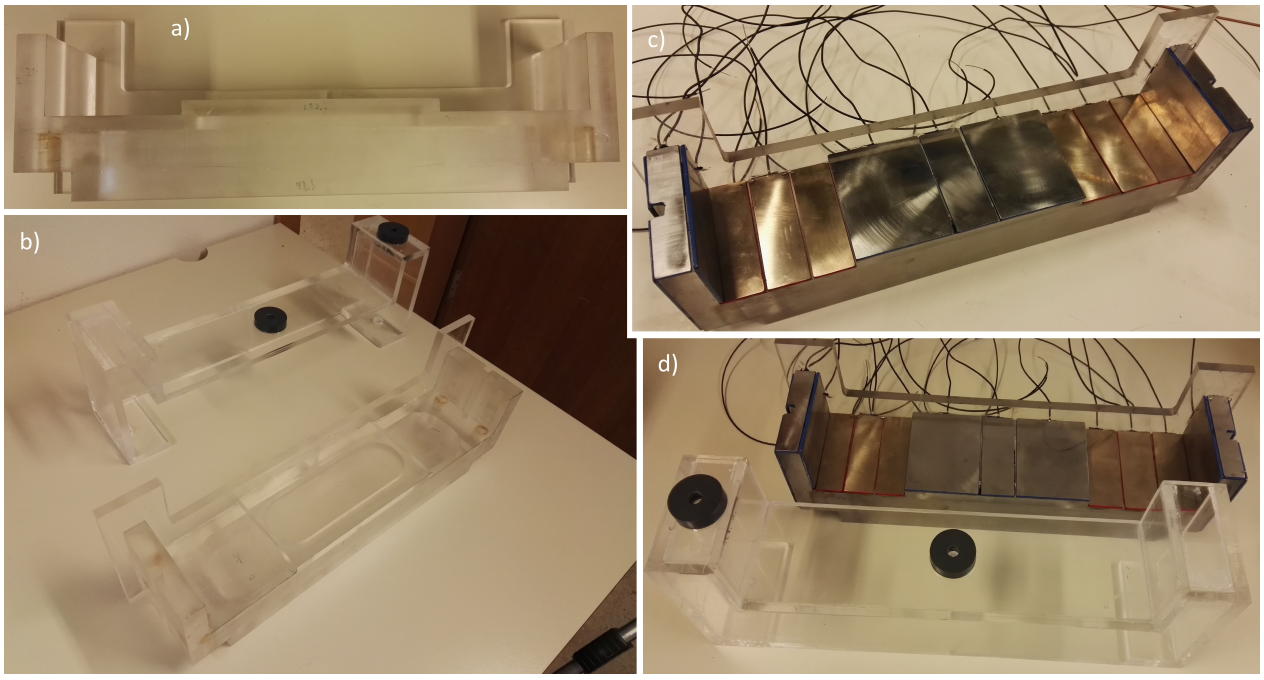

Figure 4.1: a) acrylic structure, b) both parts of the test cell, c) metal samples adhered to the acrylic, d) test cell prior to closing.

The test cell is constructed on the basis of symmetry in the thruster. This test cell is $\frac{1}{18}$ symmetric piece of a 1:2 thruster. The original thruster is made of solid NAB and SS as illustrated in Figure 1.1, however for the experimental testing in this thesis the electrolytes interaction with the metal surface is the focus. Therefore subsurface material is not accounted for. The structure of the thruster is however important, and milled acrylic is used to illustrate the geometry of the structure. The milled acrylic structure can be seen in Figure 4.1a). To properly have the correct cross-sectional water path throughout the geometry, a box by plexiglas was created to restrict the boundary of the electrolyte (see Figure 4.1b)). Figure 4.1c) illustrates how the metal samples were placed on the boundary of the acrylic piece, further illustration of how and where each sample is placed can be seen in Section 4.3. This test cell has been further modified in this master thesis and is explained in Section 4.2.

4.2 Modification of the test cell

From the project that was conducted during the previous semester, a test cell was created. This test cell was made to replicate a realistic situation, and was used to run experiments to document different scenarios with galvanic corrosion between the two metals SS and NAB. The two experiments were both run in stagnant water, and therefore implementing water flow was not an issue. However, for the experiments in this master thesis water flow was necessary. As well as the implementation of water flow, some modifications were made to the opening and closing mechanism to simplify this action.

Oxygen content inside a compartment with a limited replacement of fresh seawater was an interesting parameter. A Self-adhesive Oxygen Sensor (22) was added to measure the oxygen content inside the test cell. A PreSens Fibox LCD 3 Oxygen measuring tool (23) was necessary to read the oxygen content from the sensor. This tool would not be able to measure the oxygen level throughout the testing period, but would require manual measurements. A glass cylinder with a measuring sensor on the end was fitted through the plexiglas from above. The other end would have to be above the water surface, so water would not drain into the tube. Other than the oxygen sensor, no modifications to the test cell were necessary (except for the opening and closing mechanism) since the first test was a galvanic connection of the samples with cathodic protection in stagnant water.

For the second test, flow was important. There were two main issues with implementing flow; connection for the flow inlet and cathodic protection. For the connection of the flow inlet, a plastic hose connector was added to one of the two water inlets. In the first experiment, the samples were cathodically protected by an aluminium anode. This will not be possible after the water inlet hose

is connected, as the anode on the outside of the test cell will not be in contact with the electrolyte that flows through the test cell. It was therefore decided to use a potentiostat to cathodically protect the samples, which is a similar method to impressed current cathodic protection (ICCP). This lead to new problems on how to add a counter electrode and a reference electrode. The solution for the reference electrode was to use a separate beaker placed next to the water tup at the same water level. The reference electrode is placed in this beaker and connects a silicon hose between the beaker and the test cell. This silicone hose will have a string through it, and the hose will be filled with water. This way there's always an electrolyte path between the beaker and the spot where the reference electrode is supposed to be, similar to a luggin probe. This is illustrated in Figure 4.2 and 4.3.

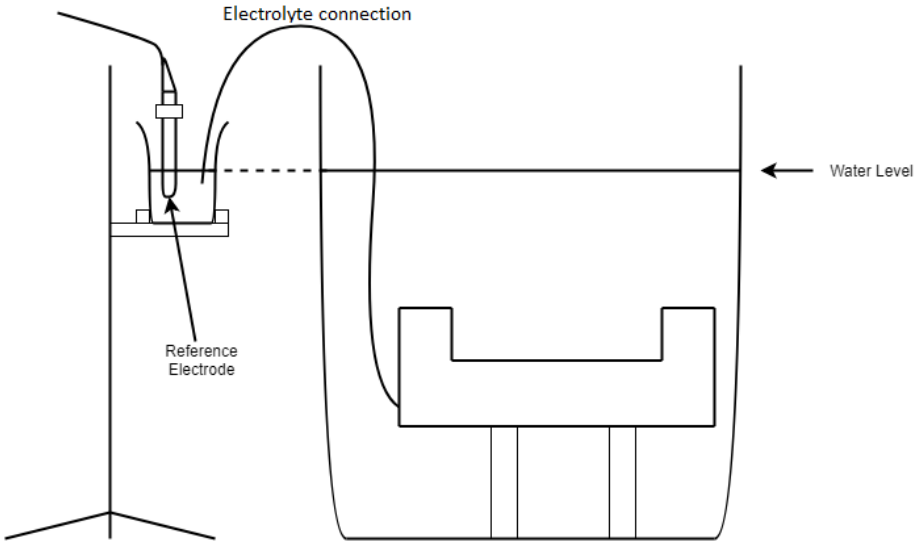

Figure 4.2: Method of placing the RE close to the CE.

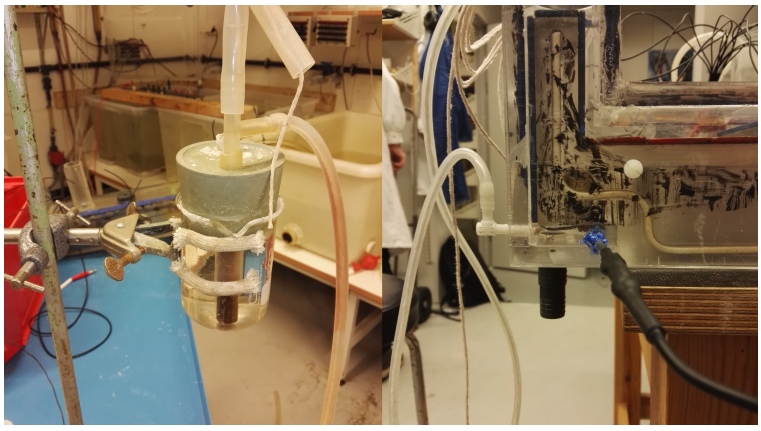

Figure 4.3: A string runs through the silicon tube between the beaker to the left, and the plastic barb connected to the test cell. The RE will be placed inside the beaker, and an electrolyte path will run through the string i the tube and into the test cell.

The second issue was the placement of a counter electrode. Ideally, this placement would be close to the water inlet as to replicate the realistic solution as best as possible. This was possible to achieve because of a open space close to the water inlet in the milled acrylic structure. This space can be seen in Figure 4.1a) in the bottom right and left corner of the structure. Two holes were drilled in the plexiglas, and a counter electrode was placed on each side. These were then connected to the potentiostat once testing began. Figure 4.4 displays the solution for the connection of the plastic hose, the connection of the silicon hose for the reference electrode and the placement of counter electrode.

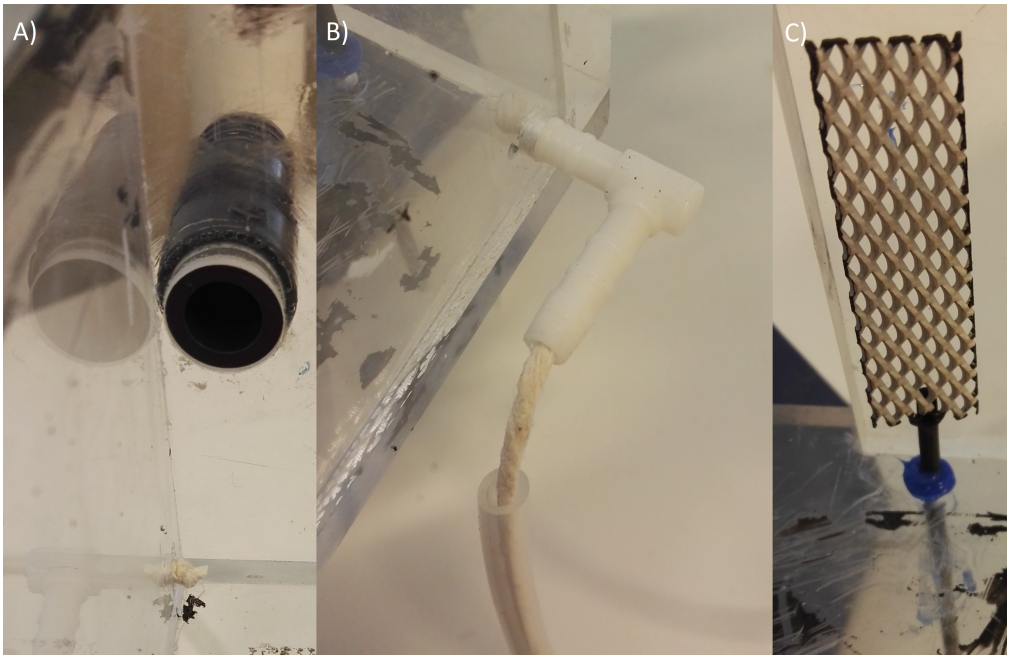

Figure 4.4: An illustration of the modifications done to the test cell to achieve the same water flow and CP. A) is on the inside of the plastic hose connector for water flow, B) is the plastic barb with a string, C) is the CE inside the test cell.

4.3 Material Setup

To accurately measure the current in each section of the PMM, the materials are separated into smaller samples. The setup for testing is illustrated in Figure 4.5 and Table 4.1.

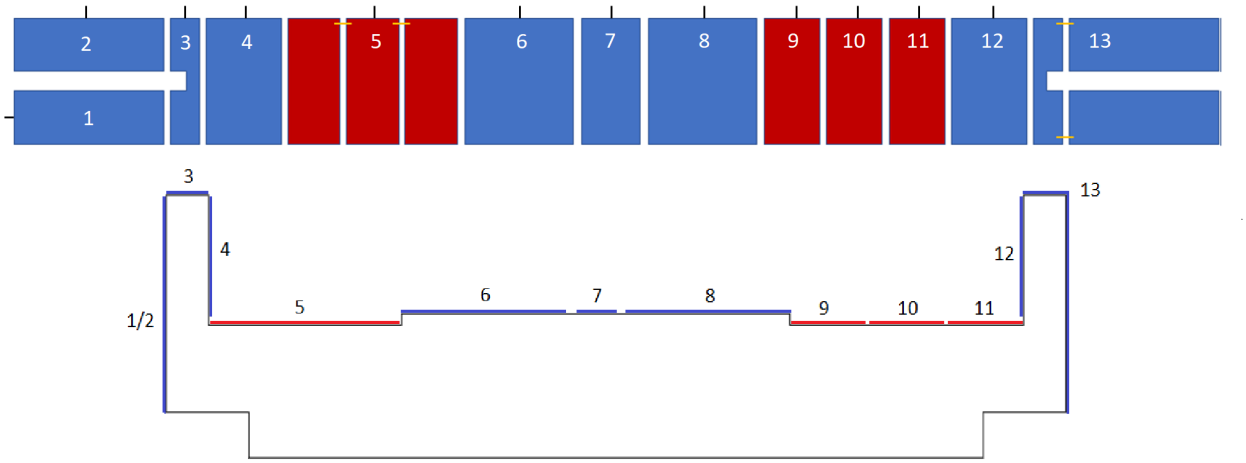

Figure 4.5: Blue samples are SS, and red samples are NAB. Setup of each material, and where each sample is placed.

Figure 4.5 illustrates the sample setup of NAB and SS, and where they are placed on the acrylic structure. Sample 5 and 13 are a connection of several samples, and are connected to investigate the behavior of larger surface areas. Table 4.1 shows which material is SS and which is NAB and the surface area of each sample.

Table 4.1: Surface area of each metal in contact with the electrolyte.

Sample	**1**	**2**	**3**	**4**	**5**	**6**	**7**
A[m^2]	0,00376	0,00376	0,001627	0,00506	0,007134	0,006624	0,00299
Material	SS	SS	SS	SS	NAB	SS	SS
Sample	**8**	**9**	**10**	**11**	**12**	**13**	**Anode**
A[m^2]	0,006624	0,003174	0,003174	0,003174	0,00506	0,008957	0,022441
Material	SS	NAB	NAB	NAB	SS	SS	Al

4.4 Experimental tests

In contrast to the experimental tests run during the preliminary project where all the tests were run in NaCl solution electrolyte (3,5% and 1%), all tests ran in this thesis are run in natural seawater. The tests are run at NTNUs Centre of Fisheries and Aquaculture (SeaLab) (24) on the dockside close to Trondheim's city center. In the corrosion laboratory at SeaLabs, there are water inlets from the wall which provide a constant supply of fresh seawater taken from 80m depth in the Trondheim fjord. Inside the corrosion laboratory, there are large plastic tubs that each have a water outlet at the top which makes it possible to constantly supply fresh seawater. These tubs are between 200-300L and different corrosion tests are run over longer periods of time. SeaLabs is a crucial asset for this thesis, and makes it possible to run as close to realistic experiments as possible.

During this thesis, three experiments were conducted; stagnant water with cathodic protection, water flow with cathodic protection and water flow without cathodic protection. The object of these tests is to determine whether it is possible to protect the metals with sacrificial anodes with regard to the potential drop through the electrolyte and geometry. Prior to test 1, all sample surfaces were ground with a level P220 grit on a grinding machine to a uniform surface roughness. Prior to test 2, the samples were not detached from the acrylic structure, as it would require extensive work and time for little to no effect. Instead, all samples were hand-ground while still connected to the structure with a level P240 grit. Between test 2 and 3 the test cell was not removed from the electrolyte, so the samples were not ground prior to test 3.

Table 4.2: An overview of the three tests completed during this thesis, the duration of each, and whether there were water flow or CP.

Test:	Objective	Temp [^{o}C]	Duration	CP	Water flow
1	Measure current consumption on each sample during cathodic protection.	10±1	34 days	Yes	No
2	Measure current consumption on each sample during cathodic protection with water flow.	10±1	22 days	Yes	Yes
3	Measure Galvanic Current from/to each sample.	10±1	21 days	No	Yes

4.4.1 Measurements

The testing data being logged in these experiments are current from each sample. This current is measured by logging the potential drop over a known resistance between the anode and the cathode. The current is then found using Ohm's law (25) by measuring and logging the potential drop over a known resistance, and then calculating the current. Ohm's law states that the ratio of the potential difference between the ends of a conductor to the current flowing through it is constant, and can be calculated. The setup for measuring Δ E can be seen in Figure 4.6, and the equation for Ohm's law in Equation 4.1 (25).

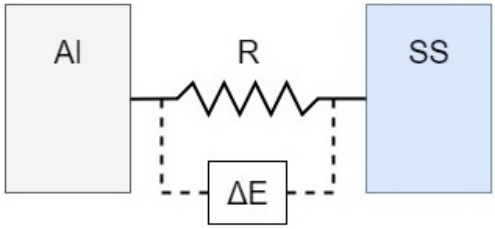

Figure 4.6: Where and how the potential drop is measured.

$$\Delta E = I * R \Rightarrow I = \frac{\Delta E}{R} \qquad (4.1)$$

Where ΔE is the measured potential drop, I is current [A] and R is the known resistance [Ω]. This potential drop (ΔE) should not be more than 2mV, because the measured result shouldn't deviate too much from the realistic values.

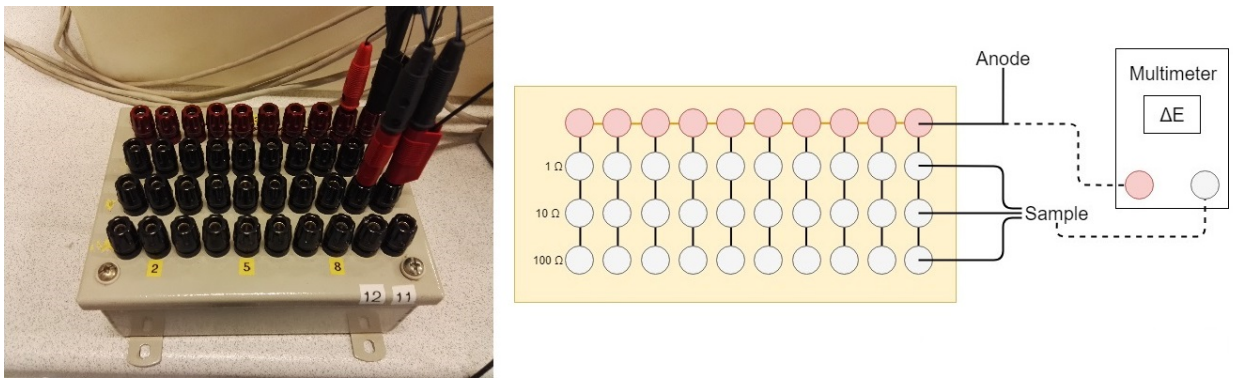

Figure 4.7: Setup of the logging equipment to measure current over time.

Figure 4.7 shows a resistance box with 1Ω, 10Ω and 100Ω resistance options. The configuration of the resistance box is also illustrated. The illustration to the right of Figure 4.7 shows the setup of current measurement of one sample. Based on the potential drop measured after initial exposure, different resistance is used.

4.4.2 Test 1: Cathodic protection in stagnant conditions

The first test conducted was cathodic protection of SS and NAB in galvanic connection in stagnant seawater. In this experiment, both SS and NAB are protected by a sacrificial anode of aluminium which is placed outside the test cell. The object of this experiment was to measure the current consumption of a bare metal surface during long periods of exposure from the anode to each segment in the test cell. An additional object to this test was to measure the oxygen content of the seawater in the confined space during exposure.

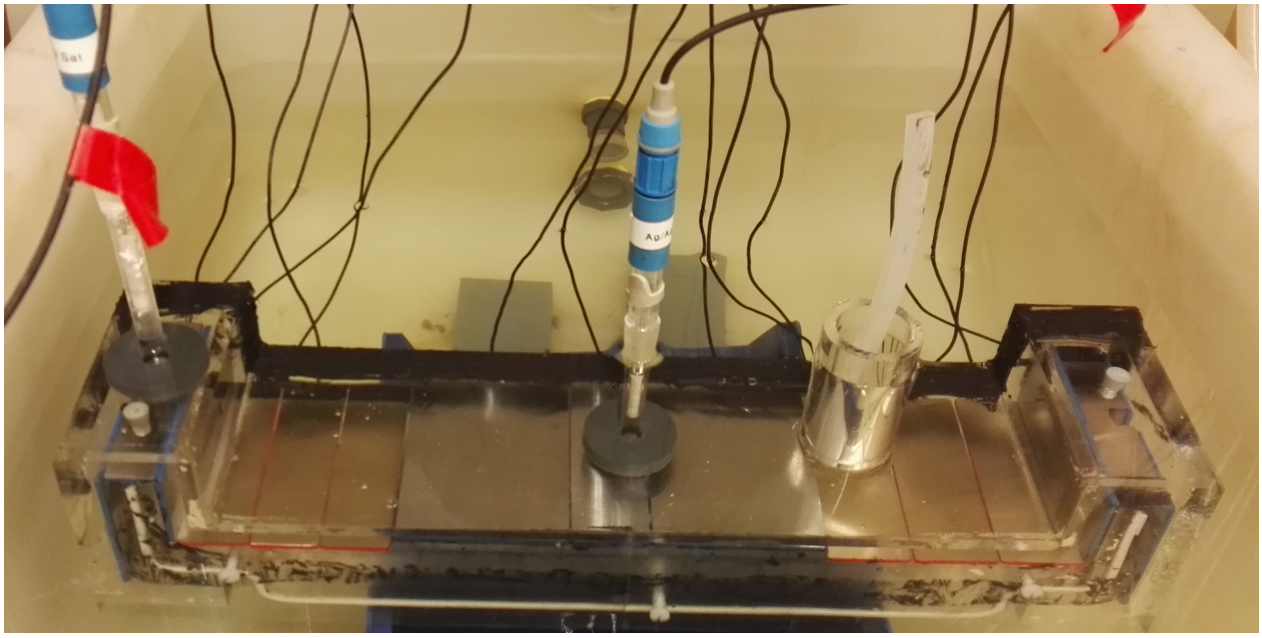

Figure 4.8: Picture taken shortly after the start of test 1.

Figure 4.8 displays the test cell after test 1 was started. The reference electrode on the left side was meant to measure the electrode potential vs. Ag/AgCl of the sample placed just after the electrolyte had passed the smallest cross-section. However, the data collected from this reference electrode were inconsistent and was therefore discarded. The reference electrode in the center measures the potential vs. Ag/AgCl of the sample in the middle of the model. This is the sample that would show the most positive potential in the test cell. The initial data collected was also inconsistent, but stabilized after a few days and was consistent until the end. The cylinder is shown to the right of the center reference electrode, and the silicon tube in the middle is the oxygen sensor. This test ran for just under five weeks.

4.4.3 Test 2: Cathodic protection with water flow

The second test conducted was cathodic protection of SS and NAB in galvanic connection with constant flow of fresh seawater. To cathodically protect the metals in this experiment, some additional modifications had to be made as is explained in Section 4.2. Because water flow was introduced to the test cell, the aluminium sacrificial anode that was used in the previous experiment would not be able to protect the samples. This is because the electrolyte that flows into the test cell comes directly from the water supply from the wall, and the electrolyte will therefore not be in contact with the anode. A potentiostat was therefore introduced and replaced the sacrificial anode from test 1.

Realistically this system will be protected using sacrificial anodes placed close to the water inlet, but since this isn't possible, a potentiostat was used. To use a potentiostat system, a counter electrode and a reference electrode has to be installed. To replicate the ideal system, the counter electrode has to be placed close to where the aluminium sacrificial anode would have been. The placement of the counter electrode and reference electrode can be seen in Figure 4.9. The finished test cell after the final modifications can be seen in Figure 4.9 and 4.10. This is a similar solution to an ICCP system.

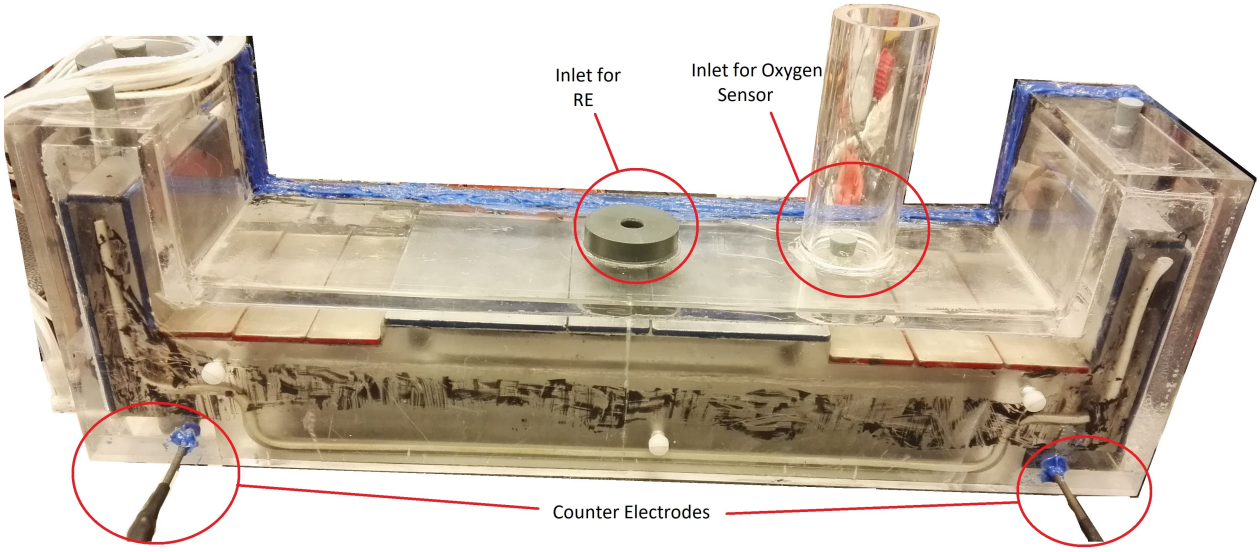

Figure 4.9: Display of different modifications done to the test cell. Counter electrode were added. The inlet for the center reference electrode and inlet for the oxygen sensor is also displayed.

Both counter electrodes can be seen inserted from the front. On each side, a silicon tube is inserted to connect the reference electrode from the outside.

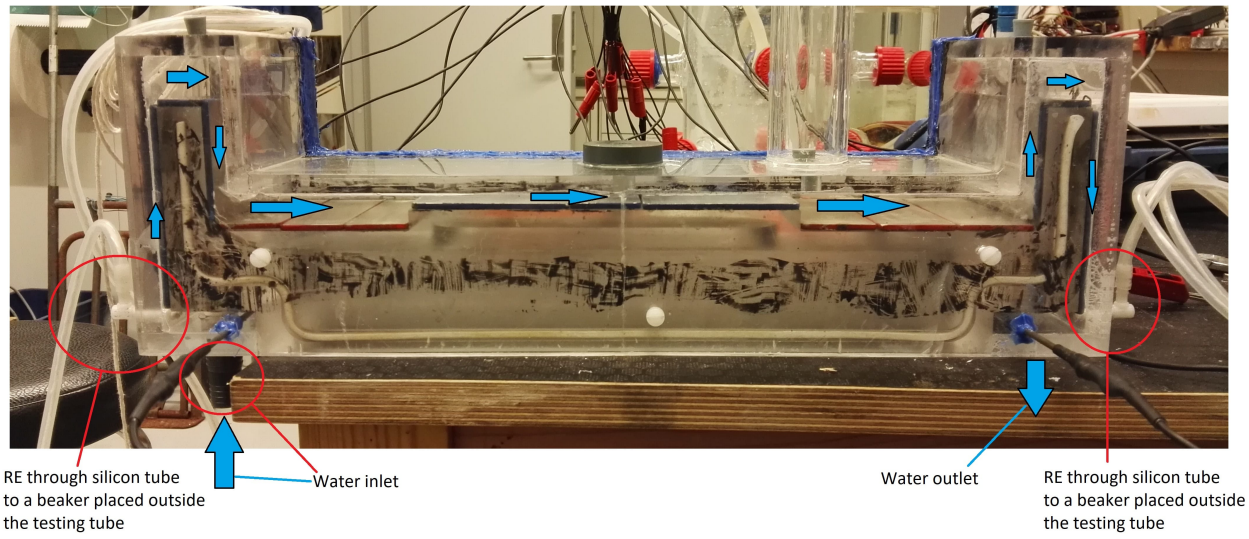

Figure 4.10: The silicone tube for the reference electrodes on each side is displayed. The water inlet and outlet is illustrated, as well as the water path through the test cell.

4.4.4 Test 3: Galvanic couple with water flow

After testing water flow with cathodic protection, the potentiostat was turned off. The test cell was not taken out of the seawater, and the samples were not re prepared for the third test. The goal was to measure the galvanic current passing between the samples of NAB and SS.

A source of error that was discovered after the last test had ended, was that during test 2 and 3, two samples were tested on the outside of the test cell. A sample of NAB and a sample of SS. During setup before testing started, an error occurred where these two samples were connected to the samples inside the test cell. This meant that the samples on the outside were in electrical contact with the rest of the samples, and in the same electrolyte. This will be further explained in Chapter 5 and 6.

4.5 Polarization Curves

Polarization curves were conducted for both types of materials after all tests. These polarization curves were then used as a boundary condition when constructing a model in COMSOL Multiphysics. These polarization curves will be displayed in Chapter 5. To record polarization curves a working electrode (WE), reference electrode (RE) and a counter electrode (CE) are required. The WE represents the metal to be polarized, the CE works as the supply of current from the potentiostat to achieve a wanted potential, and the RE represents the corrosion potential of the sample.

The polarization curves are recorded using a potentiostat to apply a current to achieve a wanted potential. The polarization curves recorded in this thesis are done after the test is finished, while the samples are still in the test cell in the electrolyte. This is done by manually setting a wanted potential, and waiting for the potential to reach steady state. The setup for recording polarization curves is displayed in Figure 4.11.

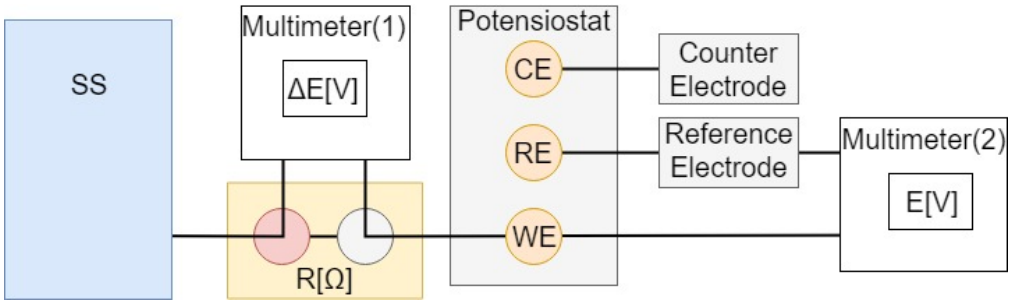

Figure 4.11: Setup of equipment to record manual polarization curves.

In Figure 4.11, the SS sample, the CE and the RE will all be in the electrolyte inside the test cell. The polarization curve recording is done by setting an initial potential of -1050mV vs. Ag/AgCl, recording the potential drop after 5 minutes, and stepwise increasing the potential by 50 mV. For test 1 and 2, all samples were cathodically protected. Therefore only the cathodic polarization curves were recorded. For test 3 the same polarization procedure was done, however, the samples were also polarized in anodic direction. For test 1 the polarization curves were run stepwise in 50 mV intervals in positive direction from -1050 to -300mV vs. Ag/AgCl. For test 2, SS was positively polarized to +100mV vs. Ag/AgCl, while NAB was polarized to -150 mV vs. Ag/AgCl. For test 3 the CP was disconnected, so the polarization curves recorded from a negative polarization potential of -500mV vs. Ag/AgCl and was stepwise positively polarized to +300mV and +150mV vs. Ag/AgCl for SS and NAB respectively. In Figure 4.11, multimeter 2 records the potential on the metal sample, while multimeter 1 records the current ($I = \frac{\Delta E}{R}$).

CHAPTER 5

RESULTS

In this chapter the results of the tests described in Chapter 4 are presented. The results from each test will be presented individually and explained. Each test will display testing data, pictures during testing, and COMSOL calculations.

5.1 Test 1: Stagnant water with Cathodic Protection

During test 1 the current to each metal sample was recorded. Figure 5.2 shows the cathodic current density for each sample during the testing period of test 1. The values stabilize after roughly three days and stay relatively stable throughout the testing period. After day 13 the cathodic current density of sample 3 reduces rapidly. The current of all SS samples inside the test cell also reduces, while sample 1, 2 and 13 increase. This occurred because the water level inside the test cell sunk, and the water level after day 13 was so low that the electrolyte inside the test cell and the electrolyte outside (in contact with the sacrificial anode) was not in contact. Figure 5.1 shows air inside the test cell, lowering the water level inside. Sample 3 was above water level, and the top part of sample 1, 2 and 13 was

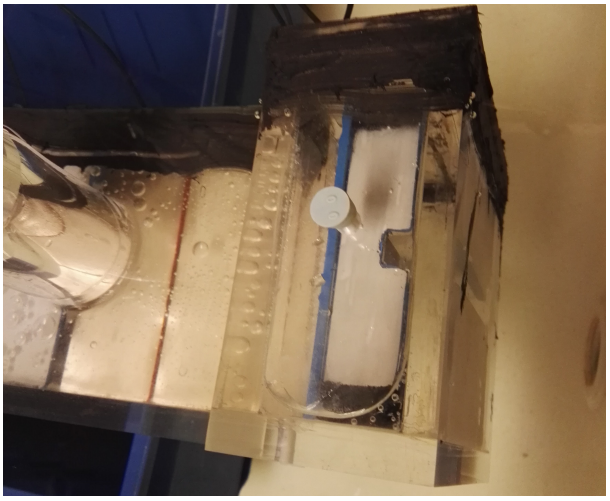

Figure 5.1: Air bubble above sample 13.

also above water. On day 14 this problem was resolved by opening a 'tap' on each side, letting water into the test cell. The cathodic current density of the NAB samples increase rapidly after new water is let in, but stabilize over the next day. From day 14 until the end, the cathodic current density on the NAB samples increases four times as can be seen in Figure 5.2. This occurs because new water is let into the test cell to avoid the previous problem. The end values of each sample at stable conditions are presented in Table 5.3. Dissolved oxygen level was measured during the first test. These values are presented in Table 5.1 and Figure 5.4. The assumption was that during the testing period, the oxygen content would reduce, which it did. However, between day 7 and 12, it increased. The theory behind this increase is that the oxygen sensor was not in contact with the electrolyte due to an air gap separating the sensor from the water.

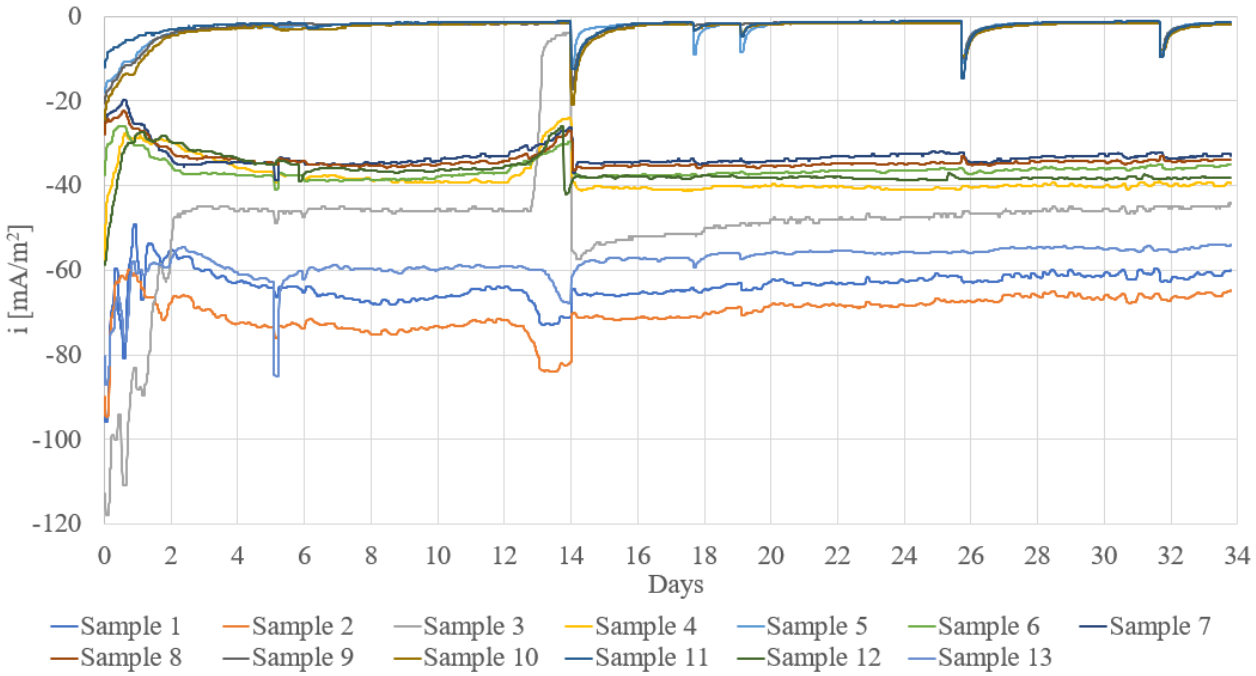

Figure 5.2: Cathodic current density for each sample through the testing period of test 1.

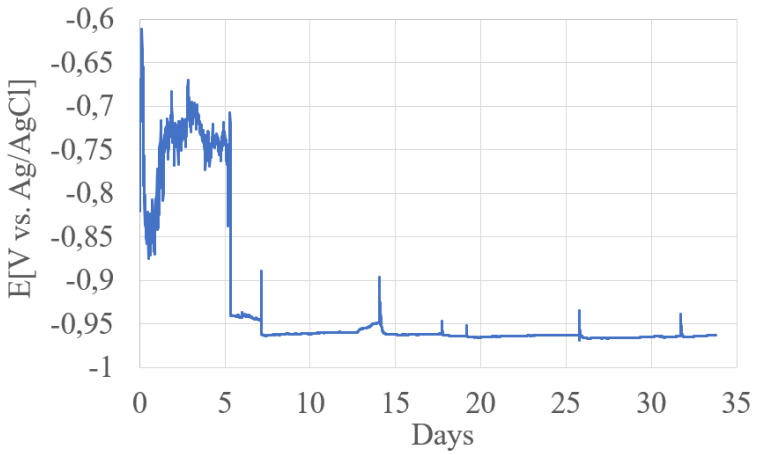

Figure 5.3: Electrode potential of sample 7 vs. Ag/AgCl in test 1.

Table 5.1: Dissolved Oxygen content inside the test cell at different intervals.

Day	[ppmw]	Temp[C]
0	9,76	9,8
1	6,72	10,7
5	3,81	10,7
6	3,6	
11	5,37	10,3
13	4,81	10,9
26	5,67	9,2

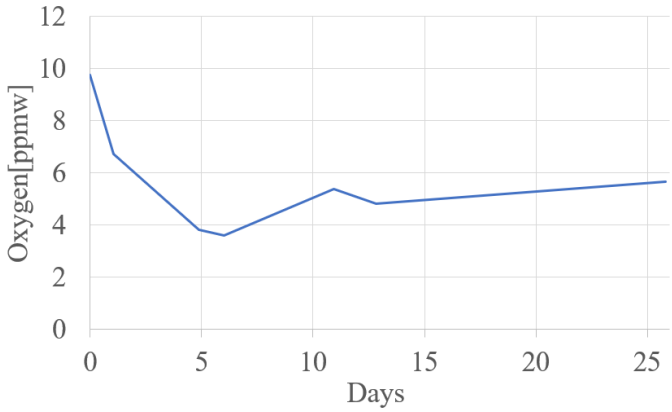

Figure 5.4: Oxygen level over time inside the test cell.

The electrode potential of sample 7 vs. Ag/AgCl is presented in Figure 5.3. The initial five days of testing shows unreliable and inconsistent data, however, after day five the measured potential on the electrode surface stabilizes. This potential will be further investigated using simplified calculations and modeling in COMSOL Multiphysics. This potential is assumed to be the most positive potential because it is furthest away from the sacrificial anode. This assumption is based on the limited space in the geometry and electrolyte resistivity through this geometry.

For calculation of the potential drop through the confined geometry, Equation 2.10 and 2.11 are used. The geometry of the electrolyte is displayed in Figure 2.4, and for this calculation, the geometry is separated into segments. Each segment has a different cross-sectional area for the electrolyte and is calculated by the height from the sample to the plexiglas boundary, and the width of the test cell.

Figure 4.5 shows the material setup. This test cell is almost symmetrical, however, the length between sample 4 and 6 is shorter than the length between sample 8 and 12. For the calculation of the potential drop, the shortest distance is used, and the different segments can be seen in Figure 5.5. Segments 5 is supposed to illustrate the area above sample 6, 7 and 8, however, for the calculation of potential drop, it's only necessary to reach sample 7. In Figure 5.5, segment 5 is a representation of sample 6 and 7. Because the width of the test cell is the same through the entire electrolyte, the calculations are simplified. The interesting parameters are the height of the section (h) and the length (L). The current consumption for each section is listed (I_A), and the current passing through the segment (I_N).

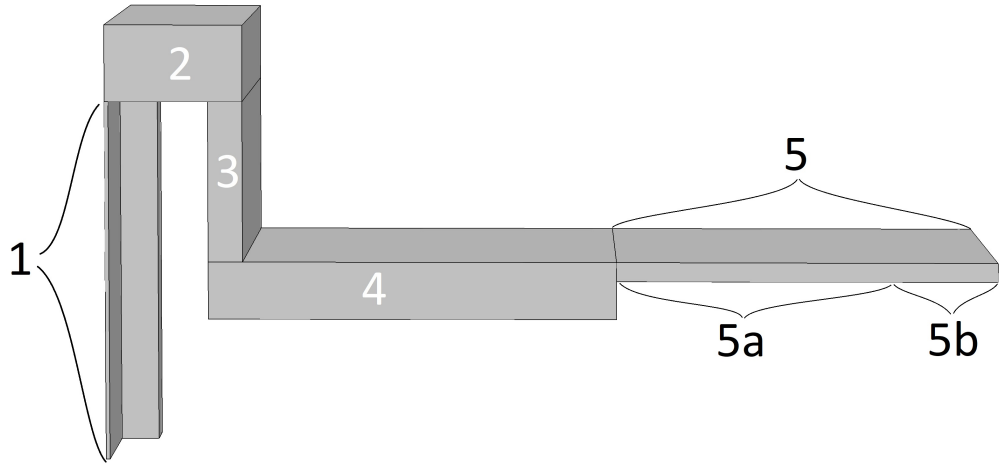

Figure 5.5: Segments used for calculation of potential drop.

The cathodic current density at the end of testing is also listed (i). These parameters are used in Equation 2.10 and 2.11 to calculate the total potential drop from the water inlet on one side, to sample 7 which is the sample furthest from the anode and assumed the most positive potential. Table 5.2 shows the results of these calculations.

Table 5.2: Calculation of potential drop through the confined geometry to the sample furthest from the anode.

Segment	h [mm]	L[mm]	I_A[mA]	I_N[mA]	i [mA/m2]	ΔE [mV]
1	2,315	31,33	0,157	1,084	62,460	43,870
	2,315	31,33	0,157	0,928	62,460	36,960
	2,315	31,33	0,157	0,771	62,460	30,051
2	19,5	19	0,072	0,614	44,130	1,830
3	8,5	55	0,201	0,543	39,625	9,333
4	15	87	0,011	0,342	1,500	7,146
5a	5	72	0,233	0,331	35,130	10,098
5b	5	32,5	0,099	0,099	33,010	1,046
			1,084			140,334

COMSOL Multiphysics was used as a tool to simulate similar steady-state conditions using secondary current distribution for a stagnant seawater experiment. A model for the electrolyte was made, and cathodic current density boundary conditions were added from the experimental test (polarization curves). COMSOL calculates the electrolyte current density vector and electrode potential for each segment. Figure 5.6 shows the potential of the boundary, while Figure 5.7 shows the cathodic current density on the surface boundary. Table 5.3 shows the current densities at the end of test 1 compared to the calculated results from the COMSOL model.

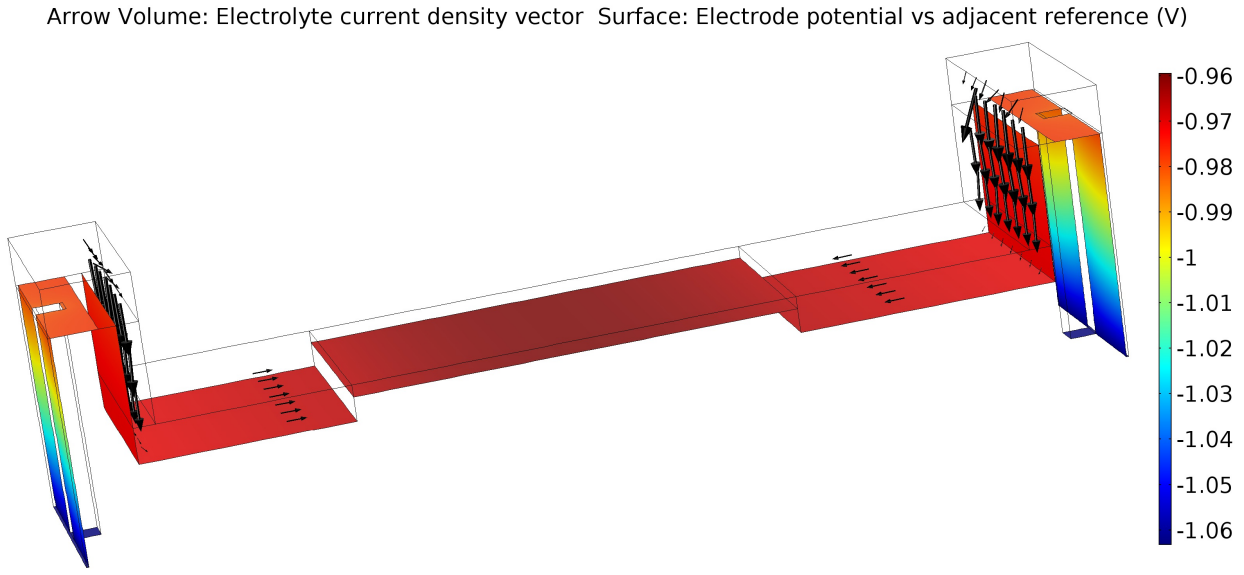

Figure 5.6: Electrode potential vs. Ag/AgCl of the boundary through the test cell during test 1.

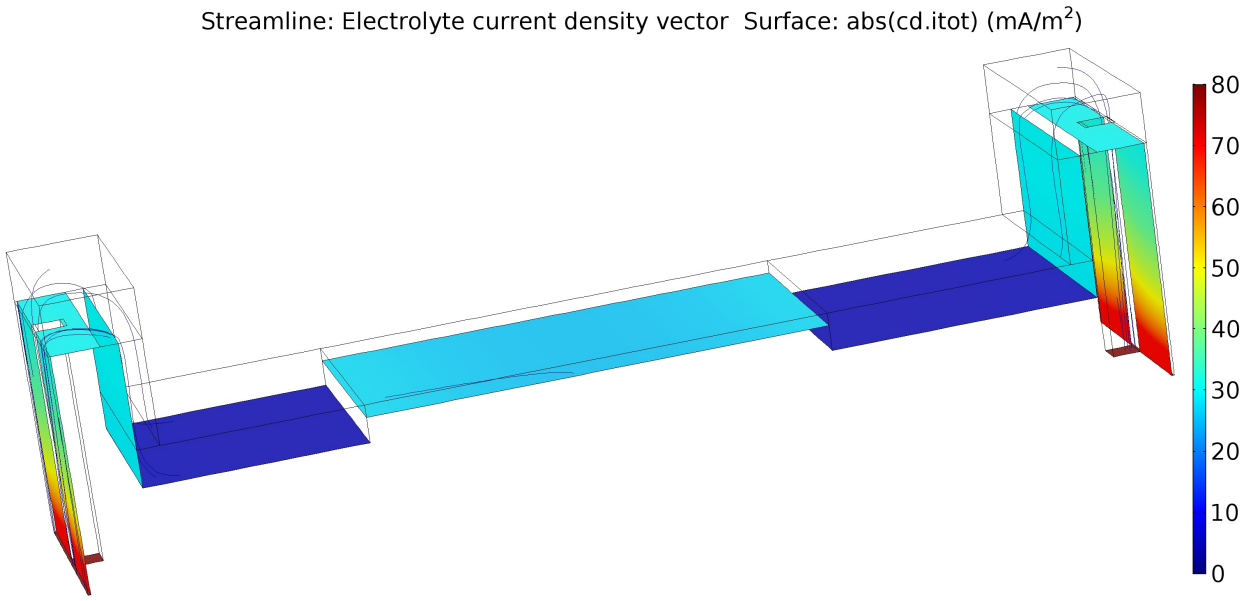

Figure 5.7: Cathodic current density in $\frac{mA}{m^2}$ of each boundary through the test cell during test 1.

Table 5.3: Cathodic current density of each sample at the end of test 1 compared to the current densities calculated in COMSOL.

Sample	Experimental i $[mA/m^2]$	COMSOL i $[mA/m^2]$	Material
1	-59,89	-69 to -31	SS
2	-65,03	-69 to -31	SS
3	-44,13	-30,3	SS
4	-39,62	-29,7	SS
5	-1,50	-4,5	NAB
6	-35,13	-26,5	SS
7	-33,01	-25,6	SS
8	-33,83	-26,9	SS
9	-1,82	-4,4	NAB
10	-1,89	-4,46	NAB
11	-1,42	-4,65	NAB
12	-38,16	-30	SS
13	-54,11	-69 to -30	SS

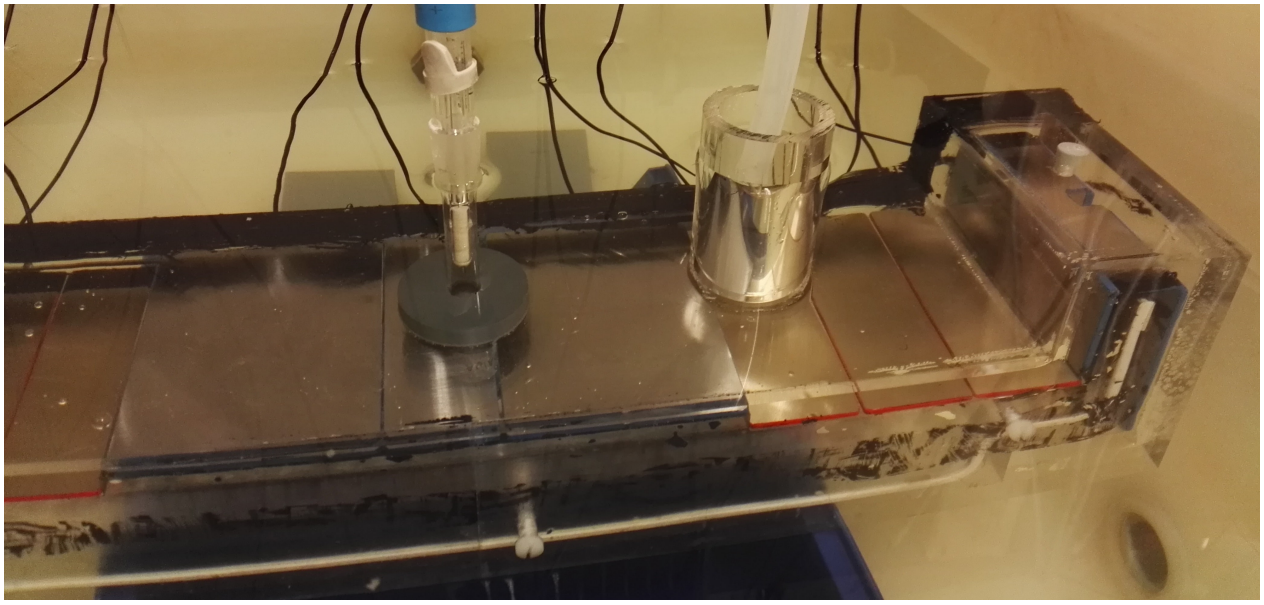

Figure 5.8: Pictures of metal samples inside the test cell initially after exposure to the seawater electrolyte.

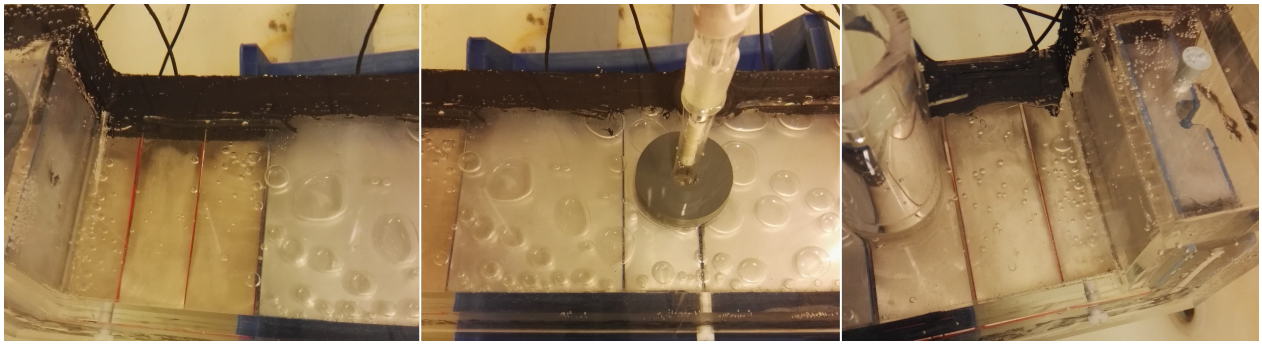

Figure 5.9: Pictures of metal samples inside the test cell after six days of exposure to the seawater electrolyte.

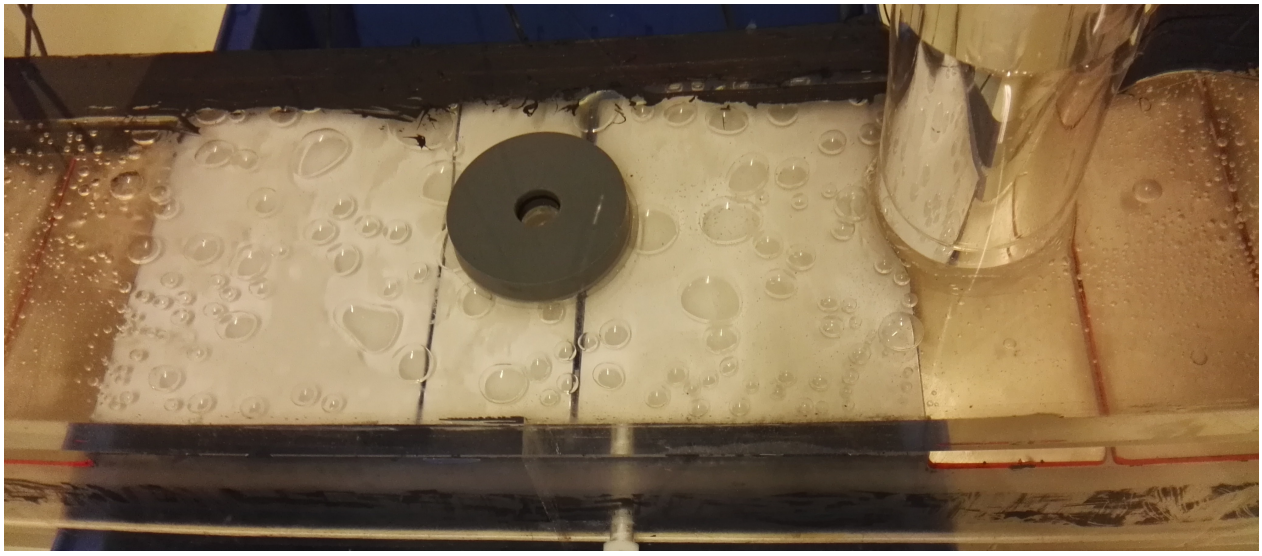

Figure 5.10: Pictures of metal samples inside the test cell at the end of exposure to the seawater electrolyte.

Pictures of the metal sample surfaces were taken during the testing period, these are presented in Figure 5.8, 5.9 and 5.10. Because of the placement inside the seawater testing tub, pictures of samples 1, 2 and parts of sample 13 could not be obtained while the test cell was in exposure. After exposure, the test cell was taken apart, and pictures were taken of the samples surfaces. Figure 5.11 shows the surfaces of all samples in the inner compartment of the test cell.

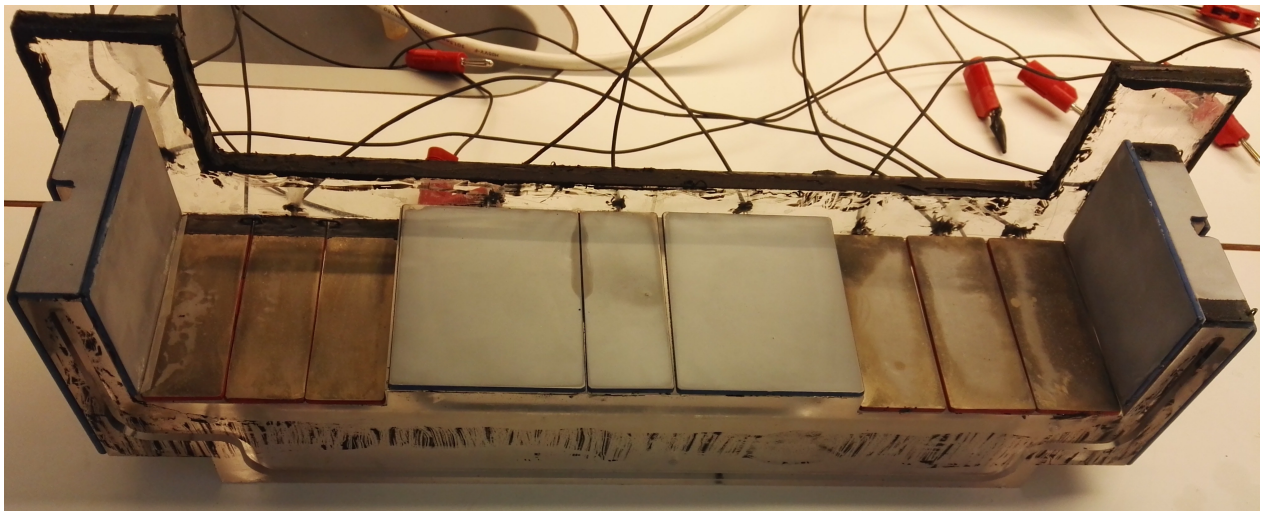

Figure 5.11: Pictures of all metal samples inside the inner compartment of the test cell after exposure.

Figure 5.12: Surface picture of sample 1, 2 and parts of sample 13. The surface has not been touched prior to these pictures. This layer is assumed to be a calcareous deposit.

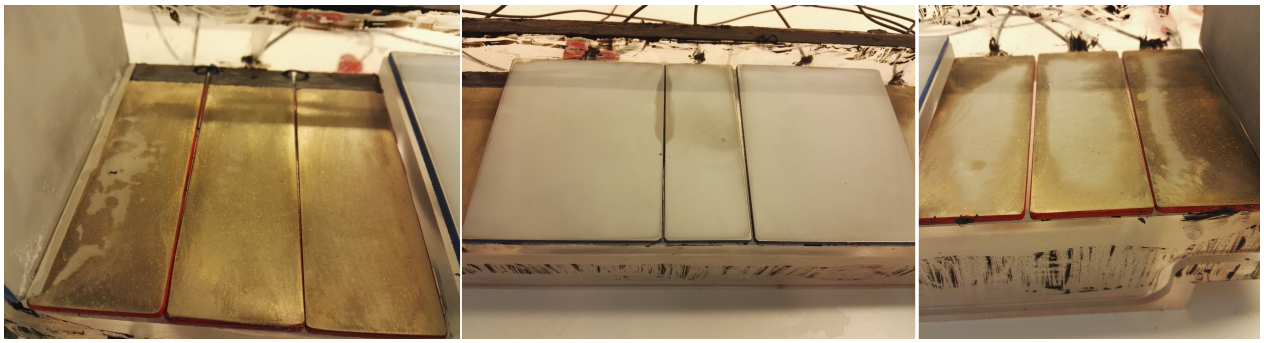

Figure 5.13: Closer look of samples 5 to 11. The SS samples in the middle had a rough grey surface, while the NAB samples had a more matte surface than prior to exposure.

5.2 Test 2: Water flow with Cathodic Protection

The same procedure was done for test 2 with samples connected to a potentiostat with water flow. Current for each sample was measured over the testing period, and are displayed in Figure 5.14. No significant error occurred during this testing. Sample 4, 6, 7, 8, and 12 have relatively low current densities for a large portion of the test. After approximately 17 days, the cathodic current density for sample 6, 7, 8 and 12 (all SS samples) started to increase, while sample 5, 9, 10 and 11 started to decrease (all NAB samples). Sample 1, 2 and 13 had relatively stable values through the testing. Freely exposed samples of both metals were added to the seawater testing tub. These were placed outside the test cell, and the objective was to measure the electrode potential simultaneously as the CP of the samples inside the test cell was conducted. A mistake was made during setup of all equipment prior to test 2. The samples outside were supposed to be connected to a reference electrode to measure the electrode potential of both samples. However, due to wiring error, these samples were connected to the samples inside the test cell and was therefore galvanically connected to the system. This was not a major concern for test 2, but the same setup was used for test 3, and those results will be provided in Section 5.3.

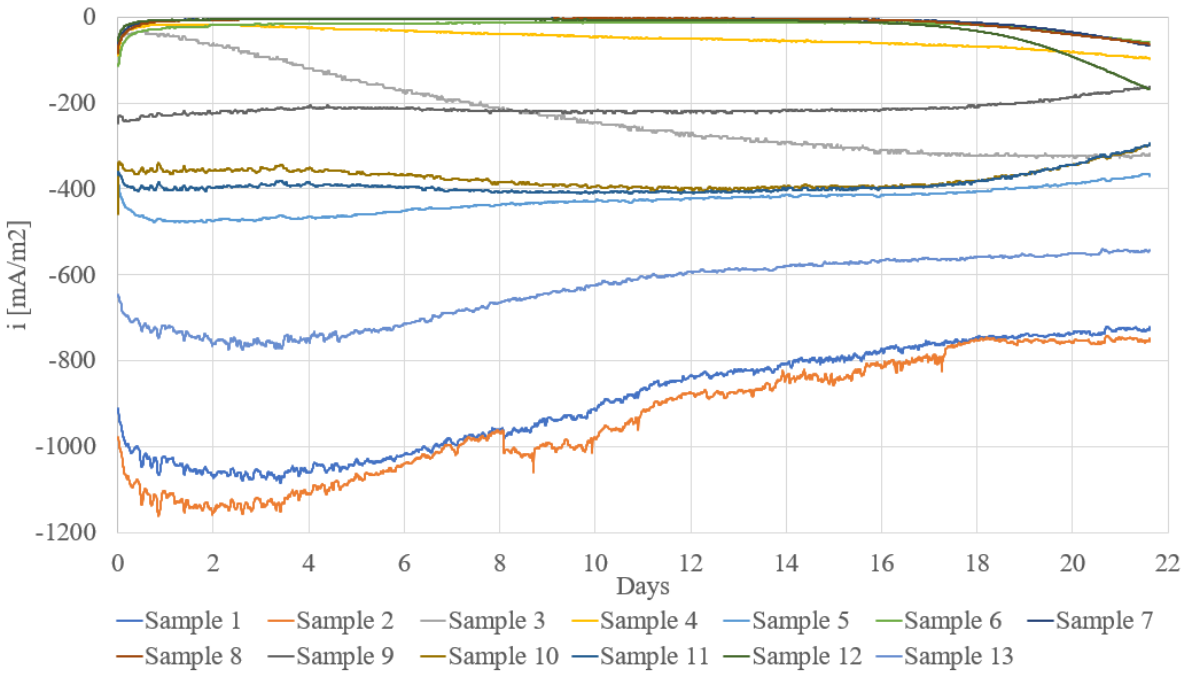

Figure 5.14: Cathodic current density for each sample through the testing period of test 2.

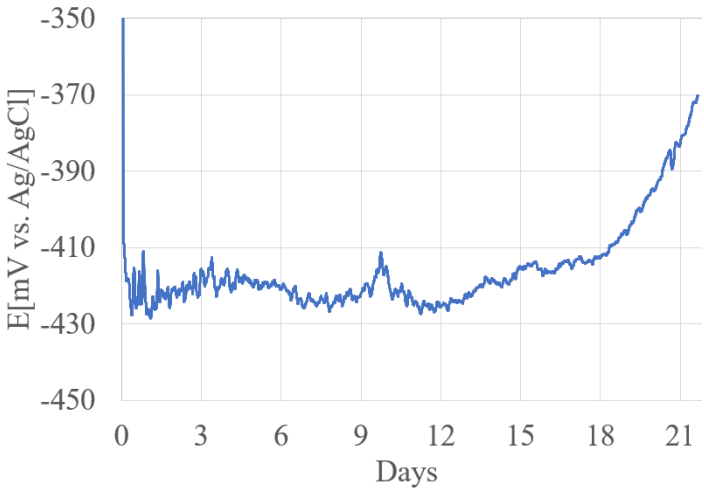

Figure 5.15: Electrode potential of sample 7 vs. Ag/AgCl in test 2.

Electrode potential of sample 7 vs. Ag/AgCl was measured for test 2. Figure 5.15 shows the electrode potential of sample 7 throughout the testing period. The potential stays relatively stable for the first 18 days before it decreases. Water flow was introduced to test 2 and 3, however, equipment to measure and control the water flow was not. Therefore manual measurements of water flow had to be made after test 3 was finished. The water flow was set after initiation of test 2 by monitoring that the water flow into the testing tub was not greater than the water flow out of it ($WF_{in} < WF_{out}$). After test 3 the hose connected to the test cell was disconnected, and the water flow was measured by filling a 5-liter measuring cup while simultaneously taking the time. Six iterations were done, and the time was listed for every liter, see table 5.4. The average time per liter was calculated, and the average cubic meter per second of water flow was calculated. Then the water flow for each segment was calculated, and the result is listed in Table 5.5.

Table 5.4: Measuring flow of water.

	Liter				
Test #	1	2	3	4	5
1		28,61	43,76	58,29	73,38
2	14,53	29,4	44,71	59,46	73,3
3	14,08	28,75	43,59	58,13	72,31
4	13,76	28,78	43,48	58,16	72,32
5	13,68	28,27	43,41	57,86	72,02
6	13,58	28,2	42,99	57,56	71,78
Avg	13,926	28,668	43,657	58,243	72,518

Table 5.5: Calculation of flow.

Average	
0,069583	$Ls^{-1}(dm^3s^{-1})$
6,96E-05	m^3s^{-1}

Table 5.6: Calculation of water speed through each segment.

Segment	Sample	A $[mm^2]$	A $[m^2]$	Flow $[m^3/s]$	Speed $[m/s]$
1	1/2/13	213	0,000213	6,9583E-05	0,327
2	3/13	1794	0,001794	6,9583E-05	0,039
3	4/12	782	0,000782	6,9583E-05	0,089
4	5/9/10/11	1230	0,00123	6,9583E-05	0,057
5	6/7/8	460	0,00046	6,9583E-05	0,151

After test 2 was finished, polarization curves were recorded on sample 1 (SS) and sample 11 (NAB), the results of this polarization curves can be seen in Figure 5.16. These polarization curves were then used as boundary conditions in COMSOL to replicate the application of flow. The results from the second test modelled in COMSOL is displayed in Figure 5.17 and 5.18. The cathodic current density is shown in Figure 5.17. Figure 5.18 shows the electrode potential of each sample through the test cell. The cathodic current density measured in test 2, and the current density calculated in COMSOL, are shown in Table 5.7.

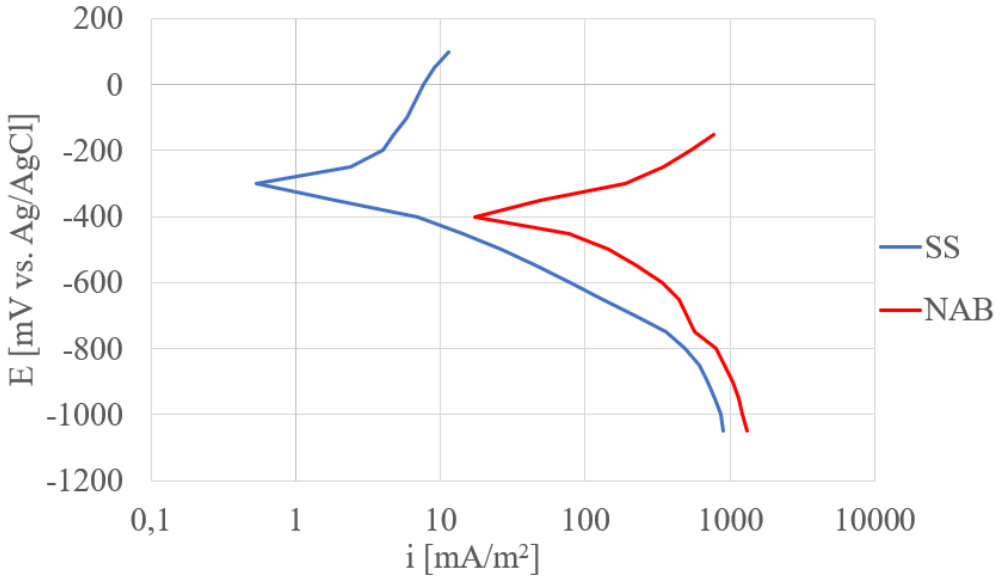

Figure 5.16: Polarization curves recorded after test 2.

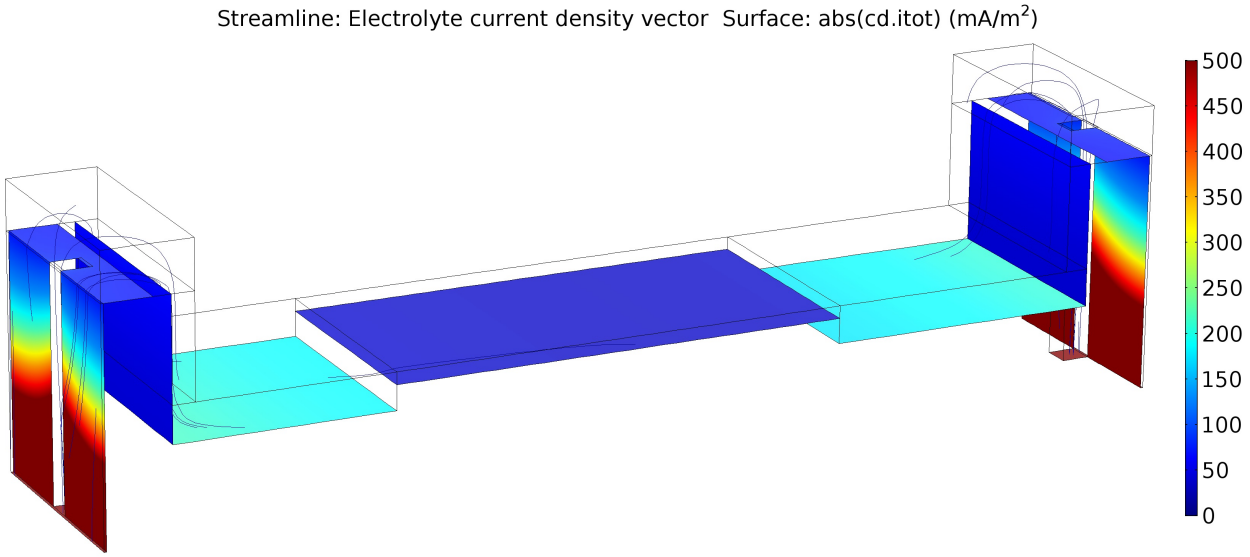

Figure 5.17: Cathodic current density through the test cell with a measurement range of 0 - 500 $\frac{mA}{m^2}$.

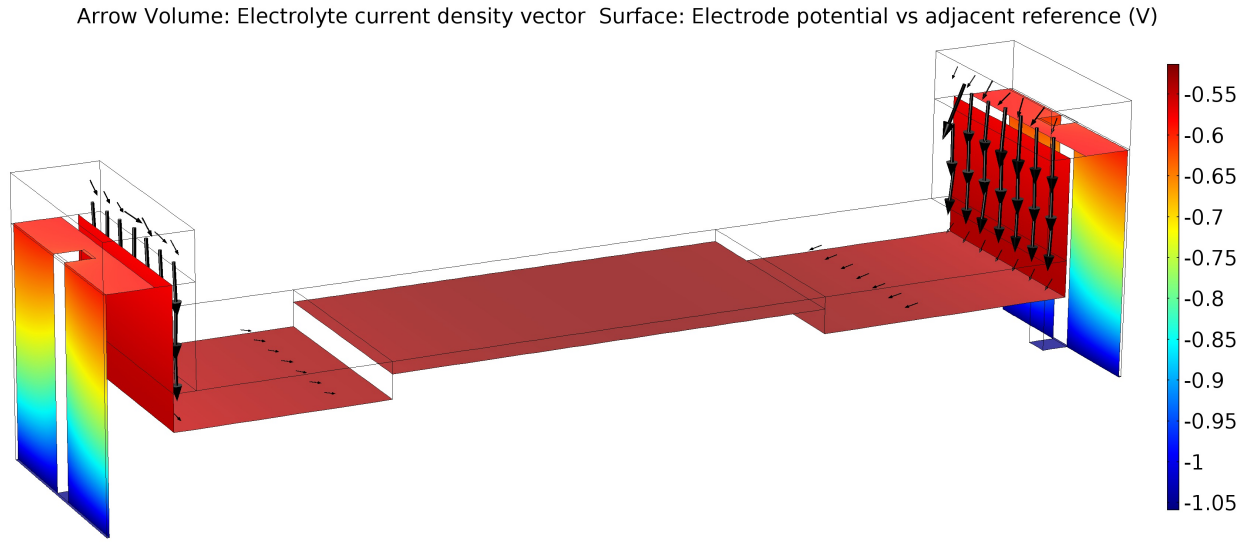

Figure 5.18: Electrode potential vs. Ag/AgCl of the surface boundary through the test cell.

Table 5.7: Cathodic current density of each sample at the end of test 2 compared to the current densities calculated in COMSOL.

Sample	Experimental i [mA/m^2]	COMSOL i [mA/m^2]	Material
1	-721,543	-888 to -88	SS
2	-747,340	-888 to -89	SS
3	-323,294	-74	SS
4	-97,431	-64 to -43	SS
5	-369,779	-218 to -188	NAB
6	-58,922	-33	SS
7	-67,425	-31	SS
8	-62,334	-32	SS
9	-162,256	-176	NAB
10	-297,417	-188	NAB
11	-293,951	-206	NAB
12	-168,281	-41 to -62	SS
13	-541,141	-68 to -888	SS

After the second test, the test cell was not taken out of the seawater exposure tub. This means that the only images of the surfaces after test 2 with water flow and CP are taken while the test cell was still immersed in seawater. These pictures are shown in Figure 5.19.

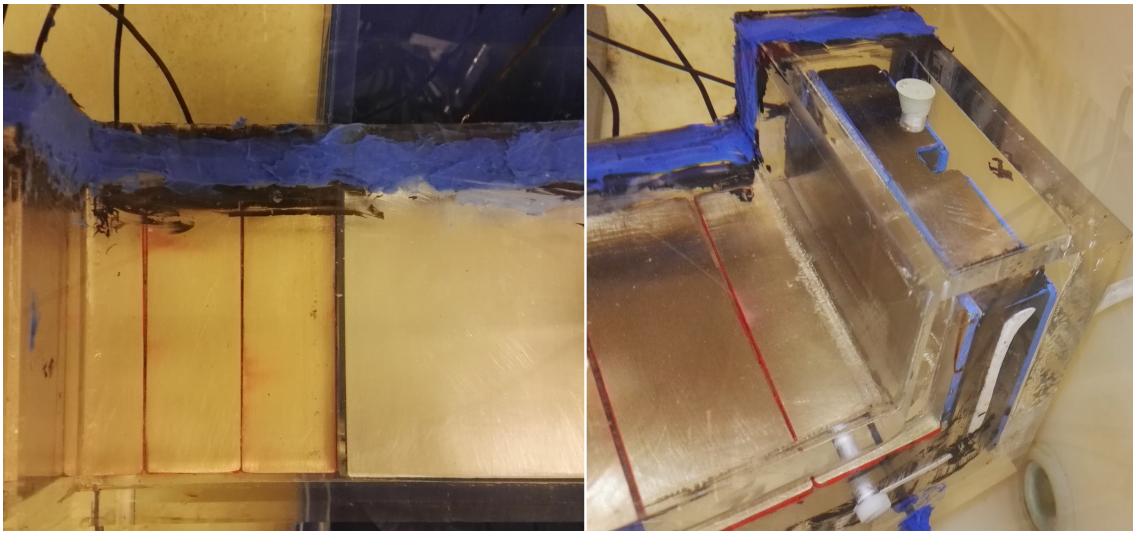

Figure 5.19: Sample surface after 18 days of exposure with CP and water flow.

5.3 Test 3: Galvanic couple with water flow

The same procedure was done for test 3. Current for each sample was measured over the testing period, and are displayed in Figure 5.20. Between test 2 and 3, the test cell was not taken apart and re-prepared for test 3. The potentiostat which provided a wanted protection potential was disconnected, and the samples were left in the galvanic couple. As has been mentioned earlier, an error occurred during setup which put the freely exposed samples of SS and NAB in connection with the samples inside the test cell. This did not affect the results as badly in test 2 since all samples were cathodically protected by the potentiostat. However, this will be further presented in test 3. The current densities measured through test 3 had some issues. Sample 1, 2 and 3 was initially connected to the other samples, however, the low values measured gave some concerns that something was wrong. They were therefore disconnected at the beginning of day 15. Between day five and six something happened to the NAB samples. Sample 11 somehow dropped from roughly 200 to below 10 $\frac{mA}{m^2}$, while sample 5 increased to over 120 $\frac{mA}{m^2}$. After day seven these variations changed back to approximately the same values as prior to the change and had stable values. The reason for these changes is unknown to the author, who could not figure out this error, or why it changed back.

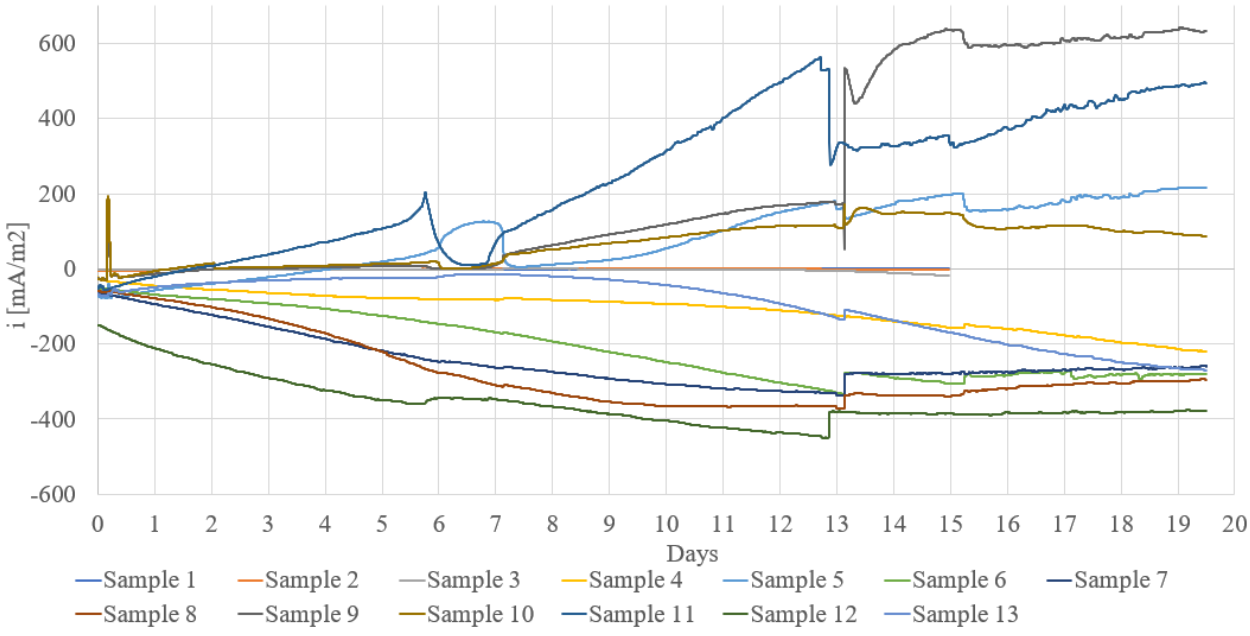

Figure 5.20: Current density for each sample through the testing period of test 3.

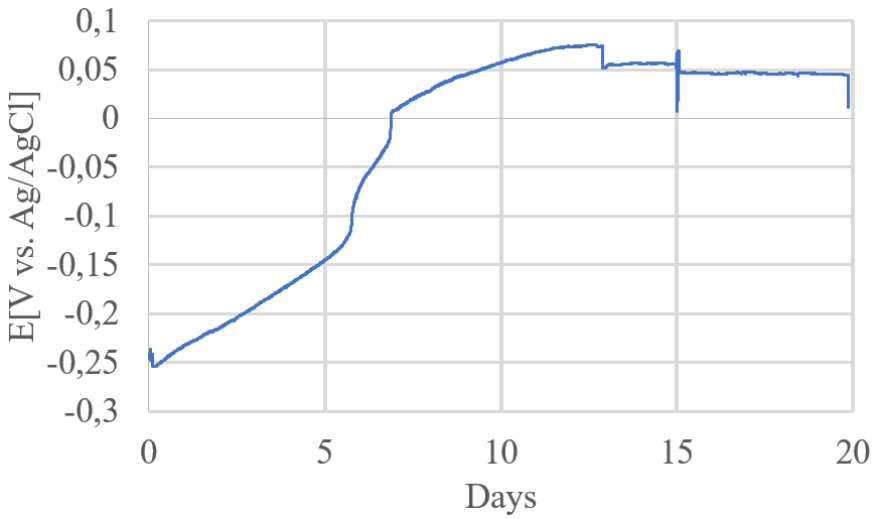

Figure 5.21: Electrode potential of sample 7 vs. Ag/AgCl in test 3.

Table 5.8 shows stable current density values at day 15, when sample 1, 2 and 3 was still connected, and at the end of the test on day 19. These values are then compared to the results with values calculated by COMSOL. Electrode potential of sample 7 vs. Ag/AgCl was measured for test 3. Figure 5.21 shows the electrode potential of sample 7 throughout the testing period. In a galvanic connection, the galvanic current produced by the less noble metal is the same as the current consumed by the noble metal. In this galvanic couple, SS is the nobler metal, and therefore: $I_{NAB} = -I_{SS}$. The total current should then be zero.

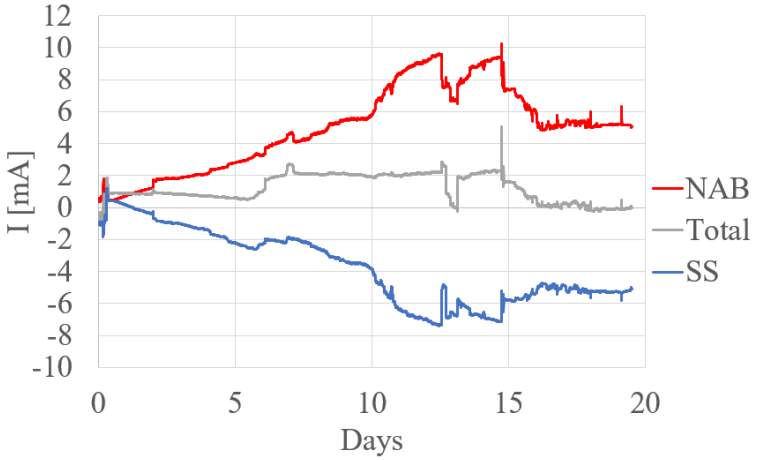

Figure 5.22: Current measured on SS samples, NAB samples, and net current in the galvanic couple.

Figure 5.22 shows the combined current measured on the NAB samples, the combined current measured on the SS samples, and the total net current. The combined current measured on the NAB

and SS samples include the freely exposed samples placed outside the test cell.

After test 3 was finished, polarization curves for both metals were recorded. The polarization curves were recorded on sample 7 (SS) and sample 10 (NAB). These were chosen because sample 7 was closest to the reference electrode, and sample 10 because it had least corrosion material covering the surface. The polarization curves recorded are shown in Figure 5.23.

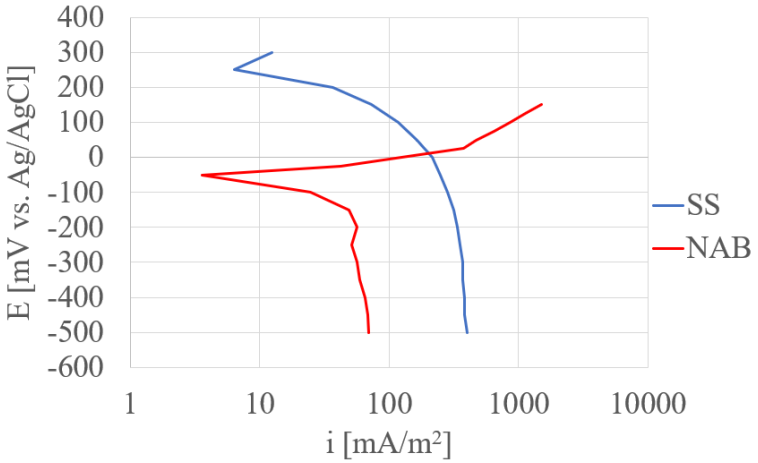

Figure 5.23: Polarization curves after test 3.

The polarization curves recorded were then used as boundary conditions for the COMSOL model, and both electrode potentials and current density is shown in Figure 5.24 and 5.25. The current measured during test 2 after day 15 (prior to removal of sample 1, 2 and 3) and after day 19, as well as current density calculated in COMSOL, are displayed in Table 5.8.

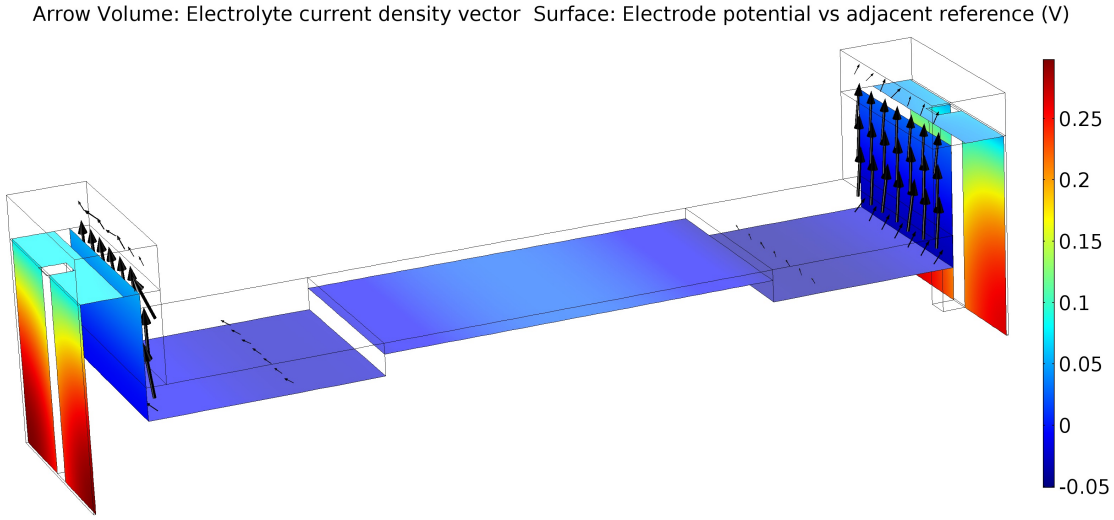

Figure 5.24: Electrode potential vs. Ag/AgCl of the surface boundary through the test cell.

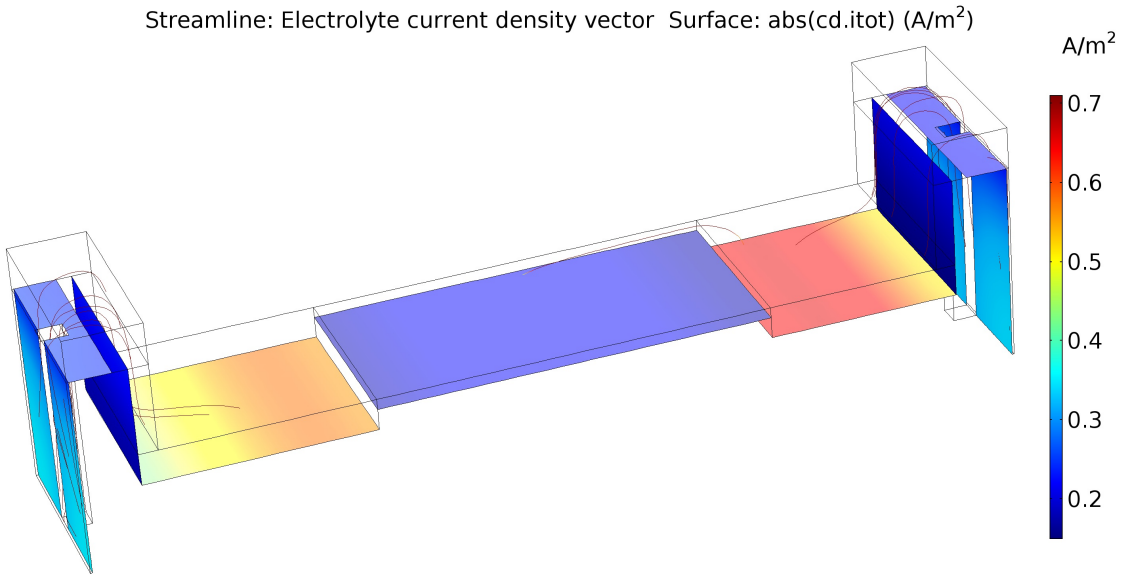

Figure 5.25: Cathodic current density on the surfaces through the test cell with a measurement range of 0.2 to 0.7 $\frac{A}{m^2}$. The direction of the current is not displayed.

Table 5.8: Experimental results from test 3 at day 15 and day 19 (the positive measurements means current from the surface, and negative measurements means current to the surface).

	Experimanetal		COMSOL	
Sample	i $[mA/m^2]$	i $[mA/m^2]$	i $[mA/m^2]$	Material
1	0,827	X	-334 to -227	SS
2	-0,484	X	-334 to -227	SS
3	-18,261	X	-220	SS
4	-155,553	-221,462	-200 to -150	SS
5	197,753	216,191	540 to 670	NAB
6	-303,907	-281,494	-170	SS
7	-278,621	-259,326	-195	SS
8	-338,745	-295,081	-180	SS
9	636,663	634,240	580	NAB
10	149,338	87,839	550	NAB
11	337,841	493,675	450	NAB
12	-384,767	-376,558	-170 to -226	SS
13	-169,442	-269,836	-340 to -237	SS

When the test cell was removed after exposure in test 3, some of the corrosion product of the NAB flushed away because of the turbulence of the water. Prior to the removal, pictures were taken of the surface of the materials inside the test cell, and are presented here. Figure 5.26 is a picture taken while the test cell is still in exposure. Figure 5.27 and 5.28 are picture taken after the test cell was opened in the laboratory.

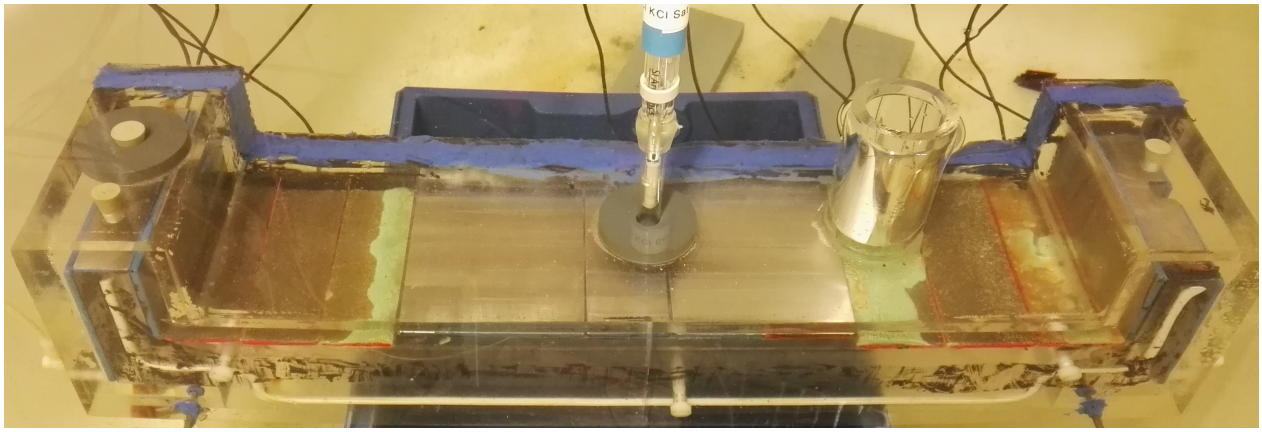

Figure 5.26: Picture of test cell still in exposure.

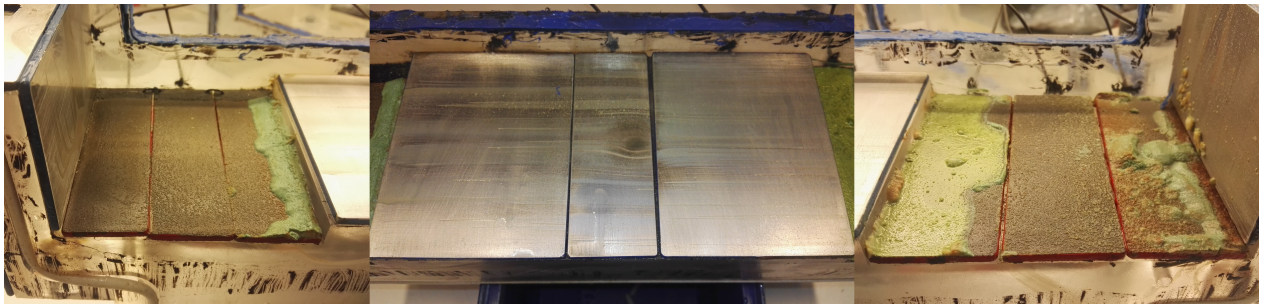

Figure 5.27: Picture of the samples inside the test cell after it was opened.

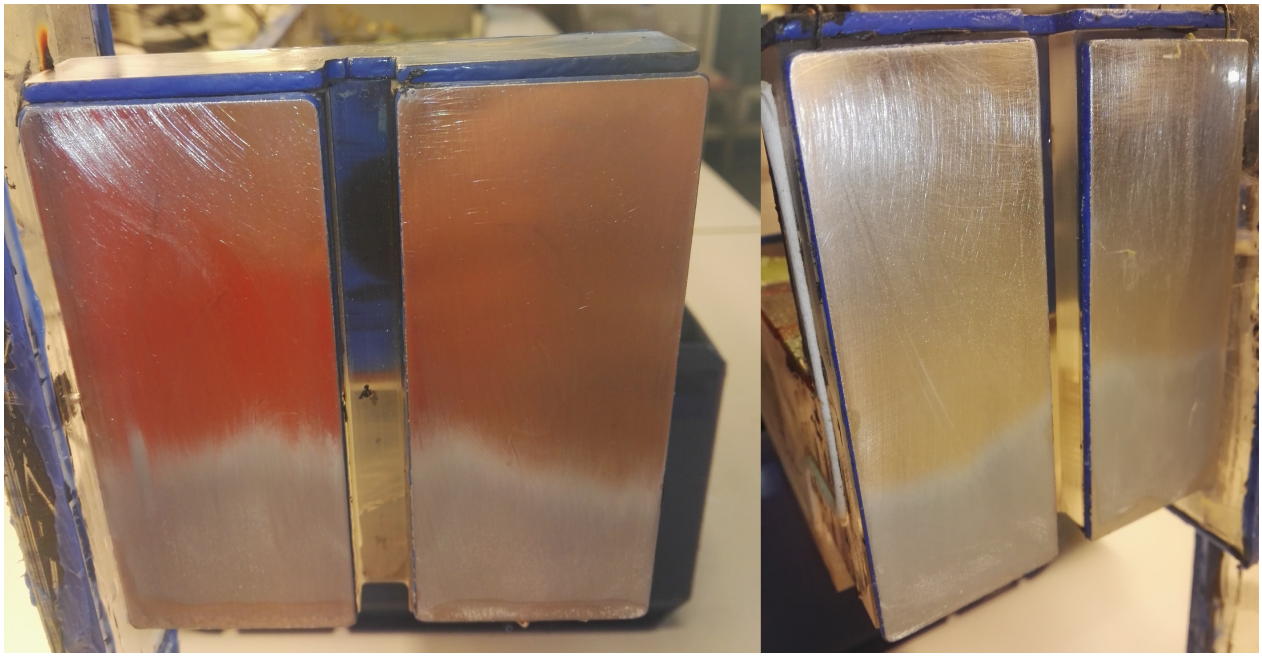

Figure 5.28: Picture of SS samples in the smallest geometry with the most confined space. The surface layer on the bottom is assumed to be a calcareous deposit. It was not possible to document a visual representation of these surfaces after test 2, so it is not known whether it developed during test 2 or test 3.

CHAPTER 6

DISCUSSION

In this chapter, the results presented in Chapter 5 will be discussed. The objective is to correlate the results from the experimental tests run in Sealab with the calculations done, and the model in COMSOL.

6.1 Potential drop through the test cell

The main objective of this master thesis was to examine the potential drop through a confined geometry and to find whether the sacrificial anode could protect the SS and NAB samples in the confined space. A potential drop will occur between the current source (anode or potentiostat) due to the current transport in the seawater in the confined space, the question is how large will it be. The hypothesis for this thesis was to find the potential drop between the aluminium sacrificial anode outside the test cell, and the sample electrode furthest from the aluminium anode. Prior to any testing, the assumption and hypothesis were made that the highest fluid resistance and the largest potential drop would occur in segment 1. The highest current will also pass through segment 1. The gap between the rotor and the stator is 1mm thick, and 94mm long. With a seawater resistivity of 0,3[Ω m], the resistance through segment 1 would be 132,4 Ω. The combined seawater resistance for segment 2, 3, 4 and 5 is calculated to be 92,5 Ω.

ISO 12473:2017 Table 2 states the potential criteria for the cathodic protection of various metals and alloys in seawater. The potential criteria for Austenitic steels (AISI 316L) with a PREN number less than 40 have a minimum negative potential of -0,50V vs. Ag/AgCl. The potential criteria for Copper alloys with or without aluminium have a minimum negative potential of -0,45 to -0,60V vs.

Ag/AgCl. This will be the electrode potential target to achieve inside the test cell. If the electrode potential inside the test cell is more positive than this, then the minimum criteria is not reached and the metal is not protected.

6.2 Test 1: Cathodic protection in stagnant conditions

In Figure 5.2 it's quite clear which values each sample stabilizes on. However, there are some changes during the first couple of days. As can be seen in Figure 5.9, six days after exposure the calcareous deposits have already started to form on the stainless steel samples. This means that between day zero and six a calcareous deposit has formed and created a barrier between the surface and the electrolyte. This barrier will reduce the current density of the metal surface. After two to three days it's possible to see the reduction of the current density of all stainless steel samples. This reduction in current density over the first few days can be explained based on the assumption of the formation of calcareous deposits.

Dissolved oxygen content was measured through the first test and can be seen in Table 5.1 and Figure 5.4. The oxygen content is assumed to reduce over time due to the oxygen reduction in the cathodic reaction, and since no new water was added to the confined space. The data shows this over the first six days, before it increases, which is assumed to be a measuring error.

Throughout the first experimental testing period, the electrode potential at samples 7 was measured, see Figure 5.3. As mentioned in Chapter 5, the potential was unreliable through the first days, but stabilized after day five and throughout the testing period. This electrode potential was -0,96V vs. Ag/AgCl at sample 7. This is an important result for the rest of the discussion about test 1, because it is the target for both the calculation of potential drop and the electrode potential in the model.

The calculations done in Table 5.2 are based on Equation 2.10 and 2.11. These two formulas can be found in Appendix A. The calculations show a potential drop through the geometrical structure to sample 7. This means that the potential measured at the sacrificial anode outside the test cell, plus the calculated potential drop would result in the assumed electrode potential at sample 7. The potential of the sacrificial anode was measured against an Ag/AgCl RE and the results can be seen in Appendix A. However, the RE was tested during and after testing and had an error of 20mV. The potential of the SA was measured at -1044mV vs. Ag/AgCl, and with a correction of 20 mV this will equate to -1064mV vs. Ag/AgCl. With the calculated potential drop, the electrode potential of sample 7 would bed: $E_7 = E_{SA} + E_{\Delta E} = -1064mV + 140mV = -924mV(-0,924V)vs.Ag/AgCl$.

This is a result relatively close to the measured potential. It is, however, important to point out that important assumptions are made that could impact this result.

In COMSOL, the geometry model is the same as the electrolyte described in Figure 3.1 and 3.2. This can be seen in Figure 5.6 and 5.7 as the thin black lines illustrate the electrolyte above the material boundary, and the colored surface illustrate the material. Figure 5.6 illustrate the electrode potential of the surface material and the direction of the current flow. The potential range is between -1,064 and -0,96V vs. Ag/AgCl because the electrode potentials calculated by the model is within this range. At the water inlet, the potential is set as -1,064V vs. Ag/AgCl as it is assumed the same potential as the SA. In the middle of the model (sample 7), the electrode potential is calculated to be -0,96V vs. Ag/AgCl. This is the same value measured during the experimental test. However, the interesting aspect is that most of the potential drop occurs through segment 1, confirming the hypothesis of the highest fluid resistance occurring through this segment. For the surface current densities, Figure 5.7 are compared to Table 5.3, where the stable values recorded at the end of test 1 are presented. The current density measured for each sample is assumed to occur on the entire surface. Table 5.3 states that sample 1 and 2 have recorded current densities of -59,89 $\frac{mA}{m^2}$ and -65,03$\frac{mA}{m^2}$ respectively, while the COMSOL model describes a gradient current density. At the bottom left and right side of Figure 5.7 the current density measured is roughly -70$\frac{mA}{m^2}$, while at the top the current density is between -30 and -40$\frac{mA}{m^2}$. The measured current density is therefore within the current density gradient along the surface.

The current density boundary conditions that were used for the COMSOL model was taken from polarization curves recorded of the materials. After test 1 polarization curves for both SS and NAB samples were recorded. However, the results were not usable because of unknown errors. Instead of these polarization curves, older polarization curves were used. During the preliminary project polarization curves for both metals were recorded in a 3,5$wt\%$NaCl solution. These curves can be seen in Appendix A. When using these curves as boundary conditions, the current density values were far too high compared to the values recorded during testing. The solution was then to reduce the current density recorded to fit the values from testing to get the COMSOL model to fit the experimental test. A rough estimate of how much each material had to be reduced was made. The NAB current density was divided by 100, while the SS was divided by 8,33 to achieve the best fit between measured and calculated potential drop. This reduction in the experimental test can be explained by the reduction in oxygen content inside the test cell, and by the formation of a surface layer.

Based on the ISO 12473:2017, with a minimum criteria of -0,50V vs. Ag/AgCl for SS and -0,45 to -0,60V vs. Ag/AgCl for NAB, the metals are cathodically protected against corrosion in stagnant conditions. Visual inspection after testing did not indicate that any form of corrosion occurred on the sample surfaces.

6.3 Test 2: Cathodic protection with water flow

The changes made in test 2 with the implementation of water flow made a significant difference in the cathodic current densities for each sample. It's still quite clear from Figure 5.14 that sample 1, 2 and 13 consume the most current. The current densities for the NAB samples have also increased, while some of the SS samples inside the test cell have remained the same. In test 1 it was clear that a calcareous deposit had formed on the samples during the first few days of exposure, but that is not the case for test 2. Test 2 also has CP which will favor the oxygen reduction and form hydroxyl ions to increase the pH on the surface which favors the formation of a deposit. However, with the implementation of water flow, these hydroxyl ions will not be able to increase the pH before the electrolyte is replaced with new fresh natural seawater. This will prevent the formation, or at least reduce the speed of deposition.

The electrode potential of sample 7 vs. Ag/AgCl of test 2 was relatively stable throughout the testing period. The value stabilized at -0,42V vs. Ag/AgCl and is the assumed protection potential inside the test cell. The potentiostat used to cathodically protect the samples was set to -1,050V vs. Ag/AgCl. This means that there is a potential drop from the CE in the potentiostat to sample 7 of -0,63V vs. Ag/AgCl. The electrode potential of sample 7 vs. Ag/AgCl will be assumed as a correct result and will be the target for the calculation and the COMSOL modeling.

Similar calculations as for test 1 was conducted for test 2, but with boundary conditions from test 2. This calculation did not yield the same similarity to the measured electrode potential as in test 1. The assumed reason for this difference is the assumptions that are made for the calculations. If the calculations were correct, the potential drop to sample 7 would be about 1050mV vs. Ag/AgCl, which would leave the electrode potential of sample 7 to be 0V vs. Ag/AgCl. This is determined to be too high of a deviation from the measured result and is neglected. The Table for this calculation can be found in Appendix A.

After test 2 was finished, polarization curves were recorded and used as boundary conditions for COMSOL. In this test, the polarization curves were used directly in COMSOL, as the values for the electrode surfaces in COMSOL were similar to those measured during the experiment. The

stable values in Table 5.7 are compared to the current densities in the COMSOL model, and the values are fairly similar. There is some deviation, but a trend and similarity can be seen. There is a current density gradient along the surface of sample 1, 2 and 13, where the current density of the surface closest to the CP is much higher than the current density of the surface furthest away. For sample 1, 2, 3 and 4 (all SS) the current density is reducing, before an increase at sample 5 (NAB). This is followed by a further reduction of sample 6, 7 and 8 (all SS). This trend is similar for both the experimental test and the COMSOL model. The trend was also seen in test 1, however with different deviations.

The electrode potential measured by COMSOL has a potential range from -1,05V to -0,55V vs. Ag/AgCl. The measured potential at sample 7 is -0,42V. Ag/AgCl, and as seen from Figure 5.18 the calculated electrode potential of sample 7 in COMSOL is approximately -0,52V vs. Ag/AgCl. This is a deviation that can be acceptable. However, it is not as accurate as the electrode potential calculated in test 1.

Based on the ISO 12473:2017 minimum criteria of -0,50V vs. Ag/AgCl for SS and -0,45 to-0,60V vs. Ag/AgCl for NAB, the protection potential with this water speed is in the grey area in terms of cathodic protection. However, the measured water speed across the sample surface is measured to be at a maximum of 33 $\frac{cm}{s}$. As mentioned in the introduction, the water speed across the surface during operations is expected to reach $30\frac{m}{2}$, which is far beyond the water speeds used in these experiments. According to the potential drop presented by the COMSOL model, it's quite clear that a large portion of the potential drop occurs through segment 1, as well as the largest current consumption is through this segment. By coating the SS and effectively reducing the current consumption significantly, the potential drop will not be as high. This will potentially be enough to reduce the electrode potential inside the test cell to a level where the NAB is protected. This is an assumption, and there has been no testing on this assumption.

6.4 Test 3: Galvanic couple with water flow

The test results from test 3 shown in Figure 5.20 do not have as clear and stable values as the previous two experiments. This can be explained by several factors. The samples inside the test cell for experiment 1 and 2 were both thoroughly prepared and cleaned prior to exposure. Test 3 was not prepared, and at the end of test 2, prior to test 3, there was a surface layer on some of the samples. This is not well documented in this report, but was observed during testing. Secondly, while measuring the ΔE over a known resistance, wanted ΔE should be below 2mV, while in this test it's set to 10mV. Due to an error on the authors part, this limit was not fully satisfied until day 13 when these changes were made. After this day, the values stabilized towards the end of the experiment. In a galvanic couple, the measured net current of the SS and the measured net current of NAB is in theory identical. This relationship in experiment 3 can be seen in Figure 5.22. The net galvanic current is zero only after day 16. Exactly why this happened is not known, but a few assumptions are made. As mentioned, after day 13 the measurements were fixed to a lower ΔE, and this could lead to a smaller error between real value and measured value. However, to lower the measured ΔE, a lower resistance had to be used, and for some samples the resistance was set to 1Ω. In the resistance box used, there was a deviation from the real resistance of $\pm$ 0,5 Ω, which in worst case could lead to a $\pm$ 50$\%$ difference between real value and the measured value. A third case is that after day 15, sample 1, 2 and 3 were disconnected because they were assumed to show incorrect values. The values measured were far to low compared to similar samples in the test cell. As mentioned, it was discovered that after the testing was complete, the two samples placed outside the test cell was in galvanic contact with the samples inside. This was not so much an error in terms of the net galvanic current, because the values measured on these samples were taken into account when calculating the net galvanic current.

Figure 5.21 shows the electrode potential of sample 7 vs. Ag/AgCl during test 3. The potential measured shows the same development over time as Krogstad (2) showed in her article about corrosion of NAB, and the effect of the galvanic couple to SS (the graph is also shown in Figure 2.11). She concluded that a galvanic couple of NAB to SS has the similar coupled potential to that of freely exposed NAB during the first five days, before a steep increase in galvanic potential. This steep increase was caused by the formation of biofilm on the surface of the SS samples.

The polarization curves recorded after test 3 was used in the COMSOL model, however, both the SS and NAB curves were multiplied by 0,5. This was done to get close to similar results as the experimental test. One of the assumed reasons for this reduction is that the surface area of some of

the samples has been reduced due to corrosion product, especially the NAB samples.

Figure 5.24 shows the electrode potential for the galvanic couple. In this test, the CP is disconnected, and there will therefore not be a similar potential drop gradient through segment 1. In this galvanic couple, NAB will be the less noble metal and will cathodically protect the noble metal SS. The NAB will provide current for the SS samples, and the samples in segment 1 will be furthest away from the NAB. This is why the potential in segment 1 is the most positive.

It is clear that a corrosion product is developed on the surface of the NAB samples. Krogstad (2) discovered a similar corrosion product on NAB surface when galvanically coupled to SS. The product that has developed on the surface of the NAB samples was only visually inspected, and not further investigated. Based on the similar material testing setup, and similar corrosion product developed, the assumption is that the same results occurred in test 3 as it did in Krogstads experiment with galvanic coupled NAB and SS. The NAB suffers pitting corrosion underneath the layered corrosion product on the surface after roughly 10 days of exposure when coupled to SS. She indicated that the degree of galvanic corrosion between NAB and SS is dictated by the effective area ratio between the alloys, and the cathode efficiency of SS in seawater. The most aggressive electrolyte is within the pit beneath the corrosion product on the surface. The corrosion product covering the pit is loosely adhered and is easily washed away (7).

The water speed in this experiment is quite low, with a maximum water speed across the surface of $33\frac{cm}{s}$, and a water speed of $6\frac{cm}{s}$ above the corrosion product. When gently removing the test cell from the testing tub, some turbulence occurred due to the water exiting the inner parts, and with this extra turbulence, some of the corrosion products were washed off. This is an indication of how low the corrosion product has adhered. With a testing speed of $6\frac{cm}{s}$ and a peripheral speed of the real PMM of $30\frac{m}{s}$, a 500 times higher speed, it's clear that in operation, the surface corrosion product will be washed off.

6.5 COMSOL Model

The COMSOL model created during this thesis was used for every experimental test. The variation between each test was the exchange of boundary conditions. This model was created to simulate the test cell, and to computationally achieve the same results as the experimental tests. The results from each test show that the COMSOL model and the multiphysics aspect can simulate the same results to some degree. The polarization curves recorded after each test have been used, however, with some adaptation to achieve the same results as the experimental tests. This model can be further

exploited to simulate different environmental conditions, new boundary conditions, or adaptation of old boundary conditions. This can be achieved for both CP and galvanic corrosion. The geometric model can also be improved.

CHAPTER 7

CONCLUSION

Test 1 - Cathodic protection in stagnant conditions:

- For test 1 with stagnant conditions, the CP protected all surfaces inside the test cell well. The potential drop through the structure was present, but not a problem for the protection of the surfaces inside. No visual corrosion was detected after testing.
- A calcareous deposit developed on the surface within the first two days, which reduced the cathodic current density requirement for the SS surfaces.
- The electrode potential of the sample furthest away from the sacrificial anode was measured at -0,96V vs. Ag/AgCl throughout the testing period, which is well below the minimum criteria for CP of SS 316L and NAB, according to ISO 12473:2017.

Test 2 - Cathodic protection with water flow:

- For test 2 water flow was introduced, and the maximum water speed found was $33\frac{cm}{s}$. This speed was not significant, but significant enough to prevent the formation of calcareous deposits on the SS samples.
- The cathodic current densities of all samples after implementation of water speed increased, and especially for the NAB samples, where the cathodic current density increased more than 200 times.
- The electrode potential measured on the sample furthest away from the CE was -0,42V vs. Ag/AgCl throughout the testing period. This value is not within the ISO minimum requirement for cathodic protection for either of the metal samples.

- The water speed across the surface during operations is expected to reach $30\frac{m}{2}$, which is far more than the water speed used in this experiment. An assumption made is that by coating the area with the significantly largest potential drop and current consumption, this could effectively reduce the potential inside the test cell, and protect the surfaces.

Test 3 - Galvanic corrosion of NAB and SS with water flow:

- Test 3 was without CP to measure the galvanic currents between SS and NAB with water flow. SS is the nobler metal in the couple and will lead to galvanic corrosion on the NAB. The currents measured on each metal show that current production occurs on the NAB by measuring positive currents, and the current consumption occurs on the SS by measuring negative currents.

- A corrosion product developed on the surface of NAB, with a grey/black powder underneath. The corrosion product on top was easily removed, and with a realistic water speed of over 100 times more than in test 3, it is assumed that this product will be washed away.

COMSOL Modelling:

- COMSOL Multiphysics was used for all three experiments using various boundary conditions for the current vs. potential relationship.

- With adjustments to the boundary conditions, the COMSOL model was able to calculate similar results as the experimental results.

- The COMSOL model gave a better view of where the largest potential drop was, and the variations in current consumption (for test 1 and 2) and current distribution (for test 3).

- With a functioning COMSOL model, further investigation and testing can be done. This could be higher water speeds with or without CP.

CHAPTER 8

FUTURE WORK

- **Create new samples that fit the acrylic structure:**
  - Sample 5 is three small samples of NAB electrically connected together. A suggestion is to create one large sample that fit this area, instead of having three smaller samples connected together.
  - Some optimization of the sample setup after analyzing the results of the experimental tests. In the experiments run in this thesis, sample 1 and 2 are 94mm long and 40mm wide samples that are placed vertically along segment 1. After further analysis of the experimental data, it's clear that most of the potential drop and the largest current consumption occur on these samples. However, the magnitude of these values decreases along the surfaces. Instead of having one long sample for each of sample 1 and 2, a suggestion is two separate these into three smaller samples, that are placed along the acrylic structure in segment 1.
  - Sample 13 is a combined sample of 1, 2, and 3. These three samples are connected via wires that are hammered into the samples to form an electrical connection. If sample 1 and 2 are separated into smaller samples, then the suggestion is to leave sample 13 as individual samples, and not a connection of three samples.

- **Water flow control:**
  During test 2 and 3 water flow was added to the experiment. For this thesis, there was no solution to measure the water flow and water speed without disconnecting the test cell. By adding a tool to measure the water flow in situ, it's possible to increase or decrease the flow during testing. This is a great tool to investigate how water flow and water speed impact the current density of each sample.

- **New experiments and COMSOL Multiphysics:**

  - Run a test with a galvanic connection between NAB and SS without CP in stagnant conditions. Run a second test in the same scenario with water flow, ideally with a higher water speed than the registered water speed in this thesis. Compare the results, and investigate what the galvanic current density is between the different segments of SS and NAB, and what effect the water speed is.
  - Run new measurements of oxygen content inside the test cell in stagnant conditions and make sure that no gap can separate the oxygen sensor and the seawater.
  - Experimental work with higher water speeds to find new boundary conditions for both metals to use in the COMSOL model. The COMSOL model can also be improved.

BIBLIOGRAPHY

[1] ISO-12473:2017. General principles of cathodic protection in seawater; 2017. URL Accessed: 24.05.2018. Available from: https://www.standard.no/no/Nettbutikk/produktkatalogen/Produktpresentasjon/?ProductID=942753.

[2] Krogstad HN, Johnsen R. Corrosion properties of nickel-aluminium bronze in natural seawater—Effect of galvanic coupling to UNS S31603. Corrosion Science. 2017 jun;121:43–56. Available from: https://www.sciencedirect.com/science/article/pii/S0010938X16307491.

[3] Ashworth V. Principles of Cathodic Protection. In: Corrosion: Third Edition. vol. 2. Elsevier Inc.; 2013. p. 10:3—-28.

[4] E, Bardal. Chapter 4 - Electrode Kinetics and Chapter 7 - Different Forms of Corrosion Classified on the Basis of Appearence. In: Corrosion and Protection. Springer London; 2004. p. 35–52, 89–191. Available from: https://doi.org/10.1007/978-1-85233-845-9_4.

[5] Paul S, Shrestha S, Lee CM, Harvey MDF. Thermally sprayed aluminum (TSA) coatings for extended design life of 22%Cr duplex stainless steel in marine environments. Journal of Thermal Spray Technology. 2013;22(2-3):328–336.

[6] Meigh H. COPPER-ALUMINIUM-NICKEL-IRON SYSTEM. In: Cast and Wrought Aluminium Bronzes - Properties, Processes and Structure. Maney Publishing for IOM3, the Institute of Materials, Minerals and Mining; 2000. p. 293–322. Available from: http://app.knovel.com/hotlink/pdf/rcid:kpCWABPPS2/id:

kt00AVM7Y3/cast-wrought-aluminium/cast-aluminium-bronzes?kpromoter=Summon.

[7] Krogstad HN. Corrosion of Ni-Al bronze in seawater-immersed permanent magnet motors [Doctoral Thesis]. Norwegian University of Science and Technology; 2017.

[8] COMSOL Multiphysics;. URL Accessed: 24.05.2018. Available from: https://www.comsol.com/.

[9] M Krupa, E J Lemeiux, A Lueng, E A Hogan, V G DeGiorgi, and A Seelinger. Polarization characteristics of geometrically confined spaces. WIT Press, c/o Computational Mechanics Inc. 2005;p. 67–76.

[10] E, Sawyer L J and F , Routley A and A , Chapman D and T , Crennell J. Current density required for cathodic protection. Journal of Applied Chemistry. 1965;15(4):182–190. Available from: https://onlinelibrary.wiley.com/doi/abs/10.1002/jctb.5010150405.

[11] Nişancıoğlu K. Corrosion basics and engineering : lecture notes for the course 53523 Korrosjonslære. Trondheim: Universitetet i Trondheim, Norges tekniske høgskole, Institutt for teknisk elektrokjemi; 1994.

[12] Cramer Stephen D CBSJ. 54. Galvanic Series of Metals and Alloys in Seawater. ASM International; 2005. Available from: https://app.knovel.com/hotlink/khtml/id:kt007P7NA1/asm-handbook-volume-13b/galvanic-series-metals.

[13] Johnsen R. Cathodic Protection Compendium. 2008;3.

[14] Sarlak M, Shahrabi T, Zamanzade M. Investigation of calcareous deposits formation on copper and 316L stainless steel under cathodic polarization in artificial seawater. Protection of Metals and Physical Chemistry of Surfaces. 2009 mar;45(2):216–222. Available from: https://doi.org/10.1134/S2070205109020166.

[15] Thomason W, Fischer K. Cathodic Protection of Steel Structures in Deep Water: A Review. Proceedings of Offshore Technology Conference. 1991;p. 243–252. Available from: http://www.onepetro.org/mslib/servlet/onepetropreview?id=OTC-6588-MS{&}soc=OTC.

[16] Schüssler A, Exner HE. The corrosion of nickel-aluminium bronzes in seawater-I. Protective layer formation and the passivation mechanism. Corrosion Science. 1993;34(11):1793–1802. Available from: https://www.sciencedirect.com/science/article/pii/0010938X9390017B.

[17] Harshad Bhadeshia and Robert Honeycombe. Chapter 12 - Stainless Steel. In: Steels: Microstructure and Properties (Fourth Edition). fourth edition ed. Butterworth-Heinemann; 2017. p. 343 – 376. Available from: http://www.sciencedirect.com/science/article/pii/B9780081002704000123.

[18] Adams RO. A review of the stainless steel surface. Journal of Vacuum Science & Technology A: Vacuum, Surfaces, and Films. 1983;1(1):12–18. Available from: http://avs.scitation.org/doi/10.1116/1.572301.

[19] COMSOL Multiphysics - Corrosion Module;. URL Accessed: 24.05.2018. Available from: https://www.comsol.com/corrosion-module.

[20] Brunvoll Complete Thruster Systems;p. 18–19. URL Accessed: 24.05.2018. Available from: http://oceanist.com.tr/wp-content/uploads/2014/07/Brunvoll-AS-Complete-Thruster-Systems.pdf.

[21] Brunvoll Product Range;URL Accessed: 24.05.2018. Available from: http://www.si-technik.de/schiff/produkte/brunvoll/pdf/brunvoll-product-range.pdf.

[22] PreSens. Self-adhesive Oxygen Sensor Spot SP-PSt3-SA;. URL Accessed: 24.05.2018. Available from: https://www.presens.de/products/detail/self-adhesive-oxygen-sensor-spot-sp-pst3-sa.html.

[23] PreSens. Oxygen Measurement Tool;. URL Accessed: 24.05.2018. Available from: https://www.presens.de/products/detail/fibox-3-lcd-trace.html.

[24] NTNU and Sintef. NTNU Centre of Fisheries and Aquaculture (SeaLab);. URL Accessed: 24.05.2018. Available from: https://www.ntnu.no/sealab.

[25] Law J, Rennie R. Ohm's law;. URL Accessed: 24.05.2018. Available from: http://www.oxfordreference.com/view/10.1093/acref/9780198714743.001.0001/acref-9780198714743-e-2131.

Appendices

Appendix A

Additional information

In this Appendix additional information from the preliminary project, experiments and results are displayed.

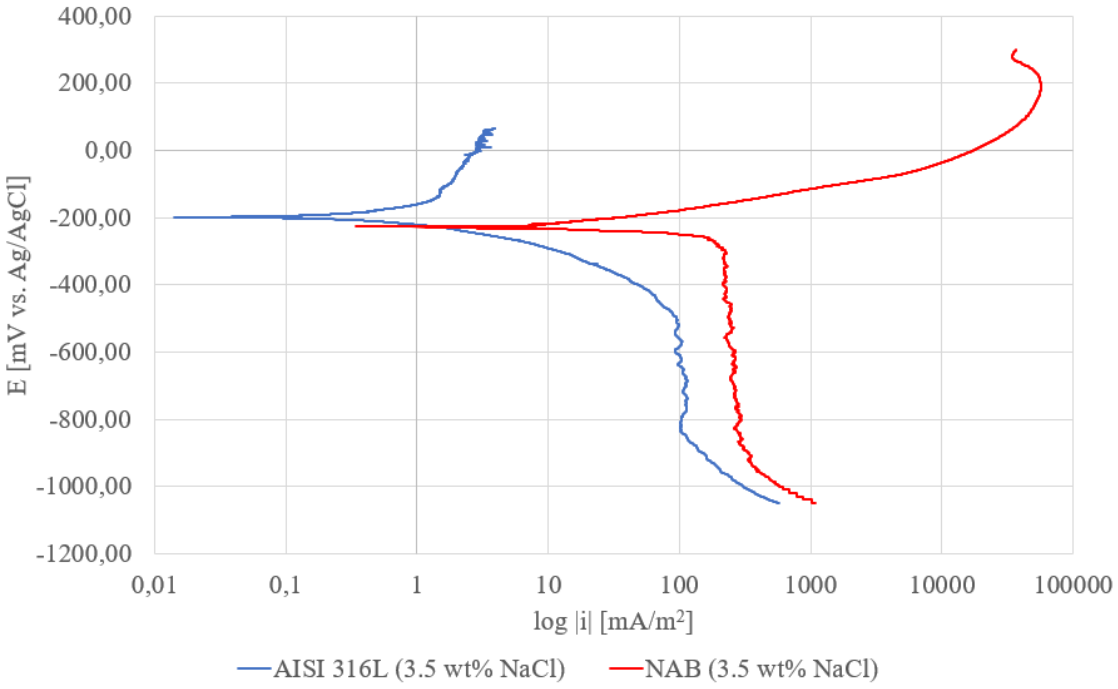

Polarization curves for NAB and SS in 3,5wt% NaCl during the preliminary project.

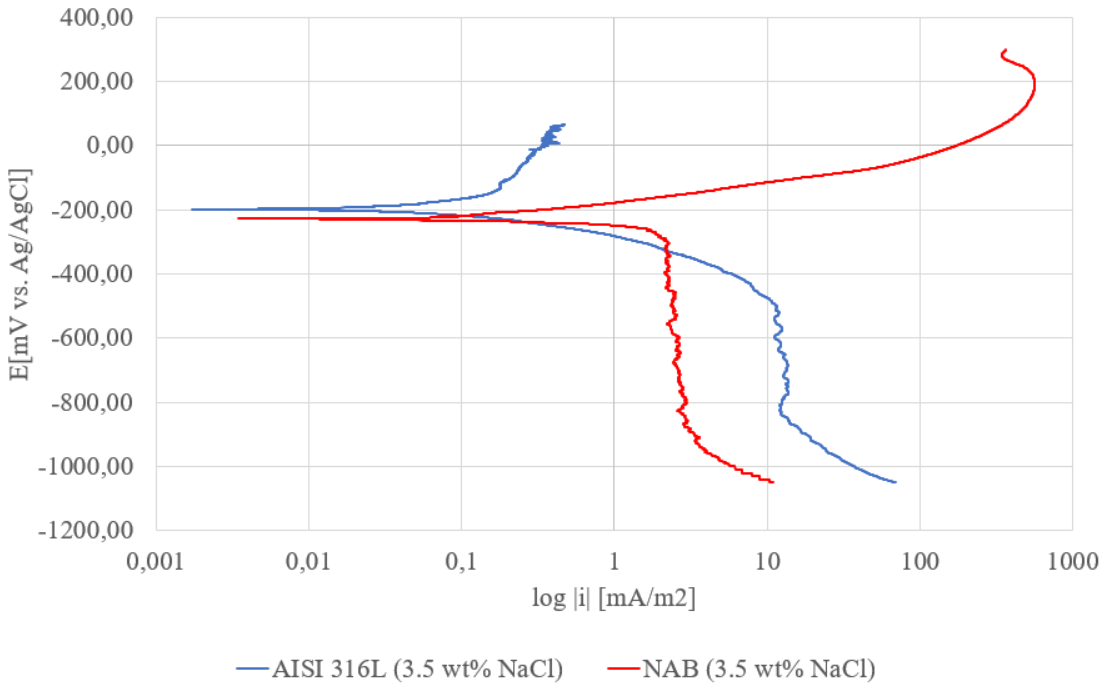

Reduced polarization curves for NAB and SS in 3,5wt% NaCl during the preliminary project.

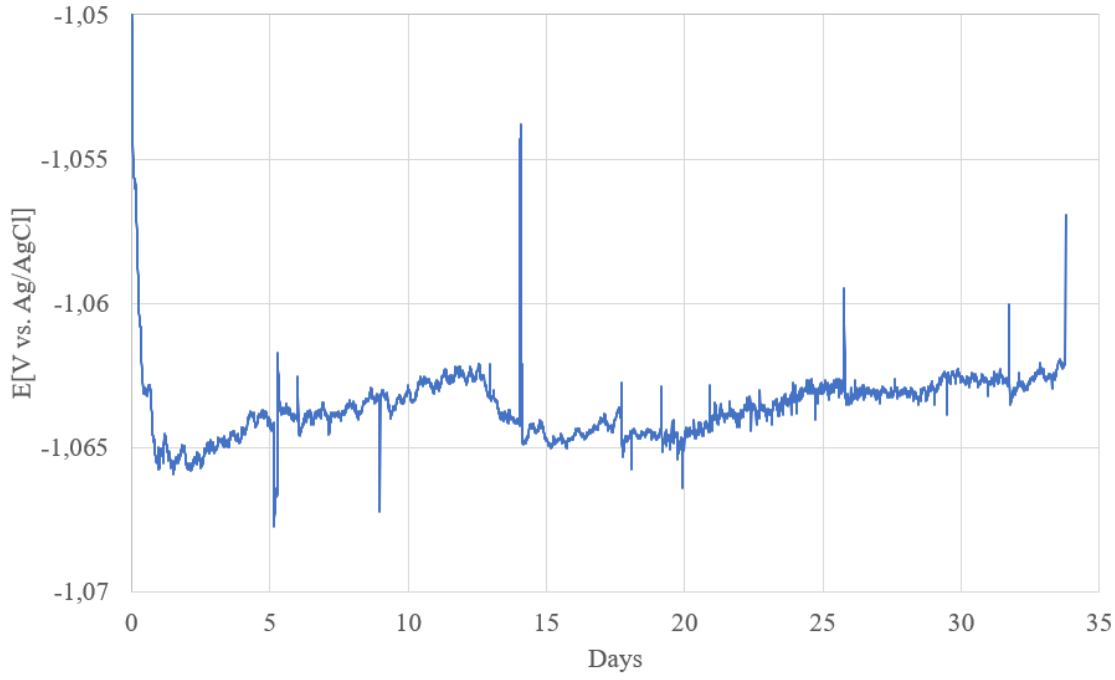

Surface potential vs. Ag/AgCl of the aluminium sacrificial anode placed outside of the test cell during test 1.

Calculation of potential drop through the confined geometry to the sample furthest from the CP, in test 2.

Segment	h	L	IA	IN	i	mV
1	2,32	31,33	1,841	9,772	734,441	384,53
	2,32	31,33	1,841	7,931	734,441	303,29
	2,32	31,33	1,841	6,090	734,441	222,04
2	19,5	19	0,526	4,249	323,294	12,60
3	8,5	55	0,493	3,723	97,431	73,35
4	15	87	2,638	3,230	369,779	33,10
5a	5	72	0,390	0,592	58,922	18,63
5b	5	32,5	0,202	0,202	67,425	1,76
			9,772			1049,30

Derivation of the formulas used to calculate the potential drop with CP.

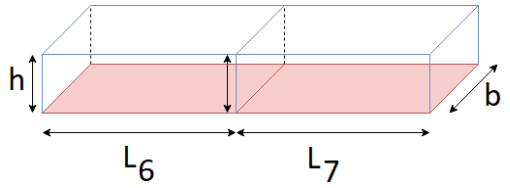

$$A' = \textit{surface area of metal} = b * L$$

$$A'' = \textit{cross section of water} = b * h$$

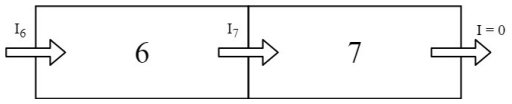

$$I_7 = i_7 * A'_7 = i_7 * b * L_7$$

$$I_6 = i_6 * b * L_6 + I_7$$

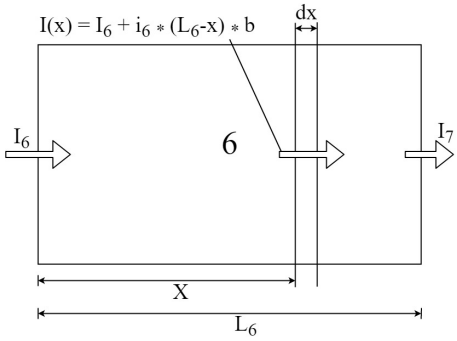

$$dE = \rho \cdot \frac{dx}{A''} \cdot [I_6 - i_6(L_6 - x) \cdot b]$$

$$\Delta E_6 = \frac{\rho}{h_6 \cdot b}[I_6 \cdot L_6 - \frac{1}{2} i_b \cdot b \cdot L_6^2]$$

$$dE = \rho \cdot \frac{dx}{A''} \cdot i_7(L - x)b$$

$$\Delta E_7 = \frac{\rho \cdot i_7 \cdot b}{2 \cdot A''} \cdot L_7^2 = \frac{\rho \cdot i_7}{2 \cdot h_7} \cdot L_7^2$$

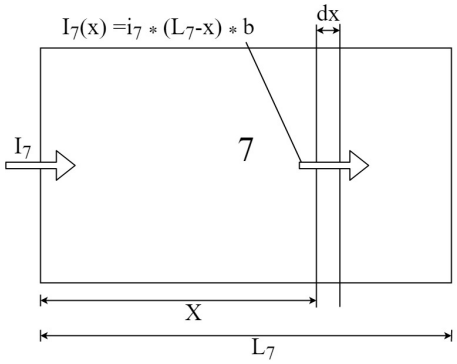

General Formulas used in calculation:

$$\Delta E_N = \frac{\rho}{h_n \cdot b}[I_N \cdot L_N \frac{1}{2} i_N \cdot b \cdot L_N^2]$$

$$N = (1 \textit{ and } 2), 3, 4, 5, 6$$

$$\Delta E = \frac{\rho \cdot i_7}{2 \cdot h_7} \cdot L_7^2$$

Appendix B

Risk Assessment for work in Corrosion Laboratory.

ID	26987	**Status**	**Dato**
Risikoområde	Risikovurdering: Helse, miljø og sikkerhet (HMS)	Opprettet	15.01.2018
Opprettet av	Simen Dyrstad Hartvigsen	Vurdering startet	15.01.2018
Ansvarlig	Simen Dyrstad Hartvigsen	Tiltak besluttet	
		Avsluttet	15.01.2018

Risikovurdering:

Corrosion Lab - Simen Hartvigsen

Roy Johnsen 11/6-18

Simen Hartvigsen 11/6-18

Gyldig i perioden:

-

Sted:

NTNU - Gløshaugen

Mål / hensikt

Jeg skal skrive masteroppgave om korrosjon, og vil benytte meg mye av korrosjosnlabben. Jeg vil benytte den til testing, og preparering av prøver og utstyr før testing.

Bakgrunn

Bakgrunnen for denne vurderingen er for ikke å komme til skade under arbeid i labben rettet mot oppgaven. Jeg benyttet meg av korrosjonslabben høsten 2017, og kjenner til den bedre nå enn på starten av høstsemesteret.

Beskrivelse og avgrensninger

Jeg blir å benytte Grinding Machine, Gemry Interface 1000 og datalogger. Blir også å benytte forskjellige redskaper som er tilgjengelig og nødvendig for mitt arbeid. Jeg blir ikke å benytte meg av farlige kjemikalier.

Forutsetninger, antakelser og forenklinger

Testene jeg skal kjøre vil gå i perioder på tre uker, men disse vil ikke bli gjort i korrosjonslabben. Vil derfor ikke bruke mye plass til mine tester i labben, men tiden vil heller bli benyttet til forberedelser til testing.

Vedlegg

[Ingen registreringer]

Referanser

[Ingen registreringer]

Oppsummering, resultat og endelig vurdering

I oppsummeringen presenteres en oversikt over farer og uønskede hendelser, samt resultat for det enkelte konsekvensområdet.

Farekilde: **Kjemikalier**

Uønsket hendelse: **Personskade**

Konsekvensområde: Helse

Risiko før tiltak: Risiko etter tiltak:

Endelig vurdering

Jeg ser på denne risikoen som liten, da det er tiltak som allerede er satt på plass for å unngå en slik hendelse. Det er viktig at disse blir etterfulgt, slik at man unngår personskader pga. for dårlig oppfølging.

Involverte enheter og personer

En risikovurdering kan gjelde for en, eller flere enheter i organisasjonen. Denne oversikten presenterer involverte enheter og personell for gjeldende risikovurdering.

Enhet /-er risikovurderingen omfatter

- Institutt for maskinteknikk og produksjon

Deltakere

[Ingen registreringer]

Lesere

Hedda Nordby Krogstad

Roy Johnsen

Andre involverte/interessenter

[Ingen registreringer]

Følgende akseptkriterier er besluttet for risikoområdet Risikovurdering: Helse, miljø og sikkerhet (HMS):

Helse	Materielle verdier	Omdømme	Ytre miljø
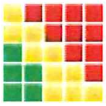			

Oversikt over eksisterende, relevante tiltak som er hensyntatt i risikovurderingen

I tabellen under presenteres eksisterende tiltak som er hensyntatt ved vurdering av sannsynlighet og konsekvens for aktuelle uønskede hendelser.

Farekilde	Uønsket hendelse	Tiltak hensyntatt ved vurdering
Kjemikalier	Personskade	Avtrekksskap.

Eksisterende og relevante tiltak med beskrivelse:

Vernebriller

Det er påbudt med vernebriller på korrosjonslabben. Dette er et tiltak som er lite plagende for brukeren, men har utrolig stor nytte. Synet skal man ha resten av livet, og har derfor stor betydning, og å bruke vernebriller er derfor et lite tiltak med stor virkning.

Avtrekksskap.

Om man benytter seg av kjemikalier som kan ha giftig eller illeluktende avdamp, må man benytte seg av avtrekksskap. Dette for ikke å skade seg selv eller andre på labben, i tillegg til at andre er klar over at det kan være giftige kjemikalier i bruk.

Risikoanalyse med vurdering av sannsynlighet og konsekvens

I denne delen av rapporten presenteres detaljer dokumentasjon av de farer, uønskede hendelser og årsaker som er vurdert. Innledningsvis oppsummeres farer med tilhørende uønskede hendelser som er tatt med i vurderingen.

Følgende farer og uønskede hendelser er vurdert i denne risikovurderingen:

- **Kjemikalier**
  - Personskade

Detaljert oversikt over farekilder og uønskede hendelser:

Farekilde: Kjemikalier

Dersom giftige kjemikalier ikke blir behandlet riktig, kan det oppstå fare for den som jobber med kjemikaliet, og andre som er tilstede på labben.

Uønsket hendelse: Personskade

Ved usikker behandling av farlige kjemikalier kan det oppstå skade på personer.

Sannsynlighet for hendelsen (felles for alle konsekvensområder): **Svært lite sannsynlig (1)**

Kommentar:

Ved eksisterende tiltak og retningslinjer satt på plass, vil alt av farlige kjemikalier behandles på en sikker måte.

Konsekvensområde: Helse

Risiko:

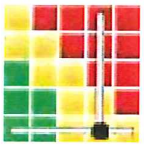

Vurdert konsekvens: **Svært stor (4)**

Kommentar: Dersom det skulle forekomme skade av farlige kjemikalier, vil dette potensielt får stor konsekvens på helsen til den det går utover.

Oversikt over besluttede risikoreduserende tiltak:

Under presenteres en oversikt over risikoreduserende tiltak som skal bidra til å reduseres sannsynlighet og/eller konsekvens for uønskede hendelser.

Detaljert oversikt over besluttede risikoreduserende tiltak med beskrivelse:

Detaljert oversikt over vurdert risiko for hver farekilde/uønsket hendelse før og etter besluttede tiltak